

Title

Dermonecrosis caused by spitting cobra snakebite is the result of toxin potentiation and is prevented by the repurposed drug varespladib

Short Title

Inhibiting necrosis caused by spitting cobra venom

Authors

Keirah E. Bartlett^{1†}, Steven R. Hall^{1,2†}, Sean A. Rasmussen³, Edouard Crittenden¹, Charlotte A. Dawson¹, Laura-Oana Albulescu^{1,2}, William Laprade⁴, Robert A. Harrison^{1,2}, Anthony J. Saviola⁵, Timothy P. Jenkins⁶, Mark C. Wilkinson¹, José María Gutiérrez⁷, Nicholas R. Casewell^{1,2*}

Affiliations

¹Centre for Snakebite Research & Interventions, Department of Tropical Disease Biology, Liverpool School of Tropical Medicine, Pembroke Place, Liverpool, L3 5QA, United Kingdom.

²Centre for Drugs & Diagnostics, Liverpool School of Tropical Medicine, Pembroke Place, Liverpool, L3 5QA, United Kingdom.

³Department of Pathology and Laboratory Medicine, Queen Elizabeth II Health Sciences Centre and Dalhousie University, 7th Floor of MacKenzie Building, 5788 University Avenue, Halifax, Nova Scotia, B3H 1V8, Canada.

⁴Department of Applied Mathematics and Computer Science, Technical University of Denmark, Kongens Lyngby, Denmark

⁵Department of USA Biochemistry and Molecular Genetics, 12801 East 17th Avenue, University of Colorado Denver, Aurora, CO 80045, USA

⁶Department of Biotechnology and Biomedicine, Technical University of Denmark, Kongens Lyngby, Denmark

⁷Instituto Clodomiro Picado, Facultad de Microbiología, Universidad de Costa Rica, PO Box 11501-2060, San José, Costa Rica.

† These authors contributed equally

* Corresponding author: nicholas.casewell@lstmed.ac.uk

Abstract

Snakebite envenoming is a neglected tropical disease that causes substantial mortality and morbidity globally. The venom of African spitting cobras often causes permanent injury via tissue-destructive dermonecrosis at the bite site, which is ineffectively treated by current antivenoms. To address this therapeutic gap, we identified the aetiological venom toxins responsible for causing local dermonecrosis. While cytotoxic three-finger toxins were primarily responsible for causing spitting cobra cytotoxicity in cultured keratinocytes, their potentiation by phospholipases A₂ toxins was essential to cause dermonecrosis *in vivo*. This evidence of probable toxin synergism suggests that a single toxin-family inhibiting drug could prevent local envenoming. We show that local injection with the repurposed phospholipase A₂-inhibiting drug varespladib significantly prevents local tissue damage caused by several spitting cobra venoms in murine models of envenoming. Our findings therefore provide a new therapeutic strategy to more effectively prevent life-changing morbidity caused by snakebite in rural Africa.

Teaser

Inhibiting PLA₂ toxicity provides a new therapeutic strategy for treating dermonecrotic pathology of local snakebite envenoming.

MAIN TEXT

Introduction

Snakebite is a neglected tropical disease (NTD) that primarily affects rural communities in sub-Saharan Africa, South/South-east Asia and Latin America, and causes an estimated 138,000 deaths per annum, with a further 400,000 people maimed annually (1). Although historically receiving little attention, in 2017 the World Health Organization (WHO) added snakebite to their list of priority NTDs and subsequently devised a roadmap aiming to halve the number of deaths and disabilities attributed to snakebite by 2030 (2).

Snakebite patients affected by local tissue damage require surgical tissue debridement or amputation to prevent the onset of life-threatening gangrene. These permanent sequelae greatly reduce the quality of life of most patients (3). Severe local pathology around the bite site results from cytotoxic, myotoxic and/or haemorrhagic venom toxins, and is most often observed after viper envenoming (1, 4). Whilst envenoming by most elapid snakes causes neurotoxic muscle paralysis and no local tissue damage, envenoming by several cobras (*Naja* spp.), most notably the African spitting cobras, causes little neurotoxicity but severe, rapidly developing swelling and tissue destruction that often leads to necrosis. These spitting cobra venoms also cause ophthalmia following defensive venom-spitting events (5-7). Spitting cobra bites are perhaps the most frequent in sub-Sahel regions of Africa and include bites by *N. pallida* in eastern Africa (8), *N. mossambica* in southern Africa (9) and *N. nigricollis* which has a wide distribution throughout northern parts of sub-Saharan Africa (10). Collectively, envenomings by spitting cobras substantially contribute to the numerous cases of severe local envenoming that result in permanent, life-afflicting morbidity across the African continent (11).

The cobra venom toxins predominantly associated with causing dermonecrotic pathology are the cytotoxic three-finger toxins (3FTx), hereafter referred to as CTx, which make up 56-85% of the total toxin abundance in spitting cobra venoms (12). CTx are well known to disrupt cell membranes and/or induce pore formation (13-15), which leads to cell death through a series of intracellular events related to the loss of control of plasma membrane permeability and via direct interaction with organelles, such as lysosomes (13, 14). Although CTx are the most abundant toxin type found in many cobra venoms (12), it is usually only those of the spitting cobras that cause severe local tissue damage after envenoming (1), suggesting that additional toxins are likely contributing to the severity of local envenoming. The next most abundant toxin family in several cobra venoms are the phospholipases A₂ (PLA₂). While the PLA₂ toxins found in elapid venoms are often neurotoxic (1), cytolytic PLA₂ also exist which can cause tissue necrosis (16, 17). For example, the spitting cobra PLA₂ nigexine is cytolytic towards multiple tumour cell lines, and reduces cell viability and cell proliferation of epithelial human amnion cells (18). It has also been proposed that toxin combinations enhance venom cytotoxicity (19-21), with PLA₂ toxins seemingly potentiating the effects of CTx (21). Understanding the relative contributions of different venom toxins to the severity of local envenoming is essential for the future design of targeted therapeutics to reduce the burden of snakebite morbidity – a key objective of our research.

Current treatment for snakebite envenoming relies on intravenous antivenom therapy, which consists of polyclonal antibodies generated via venom-immunisation of equines or ovines (1). While these therapeutics save countless lives, they are associated with a number of limitations that restrict their clinical utility, including: low affordability to those in greatest need (1, 22), limited efficacy against a breadth of snake species due to venom toxin variation (22), and high incidences of severe adverse reactions in the case of some antivenoms (23, 24). The need to deliver antivenom intravenously by a medical professional in a clinical environment prolongs the time from bite to treatment by an average of five to nine hours due to poor hospital-accessibility in the remote, rural tropical regions where most snakebites occur (22, 25, 26). Furthermore, intravenous antivenom antibodies are too large (typically ~110 or ~150 kDa) to rapidly penetrate the envenomed peripheral tissue and neutralise the aetiological cytotoxins – rendering antivenom treatment ineffective in reversing the swelling, blistering and necrotic outcomes of local envenoming (1, 22, 23, 27, 28). Collectively, these limitations highlight why the development of effective therapeutics is one of the core goals of the WHO's roadmap to reduce the impact of snakebite envenoming (2).

To address these therapeutic gaps, in this study we used a combined approach of *in vitro* cell cytotoxicity assays and *in vivo* murine models to quantify and identify the toxins responsible for venom-induced dermonecrosis caused by the most medically important African spitting cobras. Our findings demonstrate that CTx are largely responsible for cytotoxic effects observed in cellular assays using human epidermal keratinocytes but that PLA₂ toxins contribute extensively to *in vivo* envenoming pathology, by working in conjunction with CTx to cause dermonecrosis. Using the PLA₂-inhibiting repurposed drug

varespladib (LY315920) (29-31), we then demonstrate significant reductions in venom-induced dermonecrotic pathology *in vivo*, suggesting that the local injection of PLA₂-inhibitory molecules following envenoming is a viable therapeutic strategy to reduce lifelong morbidity caused by spitting cobra snakebites.

Results

Spitting cobra venoms cause heterogenous dermonecrotic lesions *in vivo*

To define the local envenoming pathology caused by medically important cobras, we intradermally challenged mice with venom from African spitting cobras. Mice were injected with two different doses of venom from east (Tanzania) and west (Nigeria) African forms of the black-necked spitting cobra (*Naja nigricollis*), which collectively exhibit a broad distribution across sub-Saharan Africa and are known to induce severe local pathology in human victims (6, 10). Following euthanasia 72 hours (h) after venom challenge, the resulting dermonecrotic lesions were excised and analysed macroscopically and microscopically.

Macroscopically, the lesions were generally heterogenous in appearance, presenting with a dark-coloured necrotic centre surrounded by a 'white' area of tissue damage (**Fig. 1A**). To better define the lesion heterogeneity microscopically, we then performed histopathological analysis on haematoxylin and eosin (H&E) stained sections of the resulting lesions (**Fig. 1B, C and D**). Sections from control mice receiving PBS only presented the typical histological pattern of normal skin, including epidermis, dermis (with skin appendages), hypodermis, panniculus carnosus and adventitia (**Fig. 1B**). When areas of venom-induced skin damage were examined, there were clear histological differences between the macroscopically white and dark regions, with more pronounced damage observed in the latter. In samples collected from the dark lesions there was extensive damage to all layers of the skin. The epidermis was lost and a hyaline proteinaceous material was observed, while the dermis and hypodermis were severely damaged with skin appendages absent. Moreover, there was widespread muscle necrosis in the panniculus carnosus (**Fig. 1C**). In contrast, the white lesions were characterised by hyperplasia of the epidermis and an inflammatory infiltrate in the dermis, together with thrombi in some blood vessels; though in general, the structure of the various layers of the skin was preserved and the skin appendages were present (**Fig. 1D**). Thus, these two different macroscopic patterns of skin lesions correspond to different histopathological scenarios. Lastly, the areas of the dark and total lesions were measured, revealing a general trend towards dose-dependent increases in lesion size, and that the area of the dark lesion never exceeded half of the total lesion area (**Fig. 1E**).

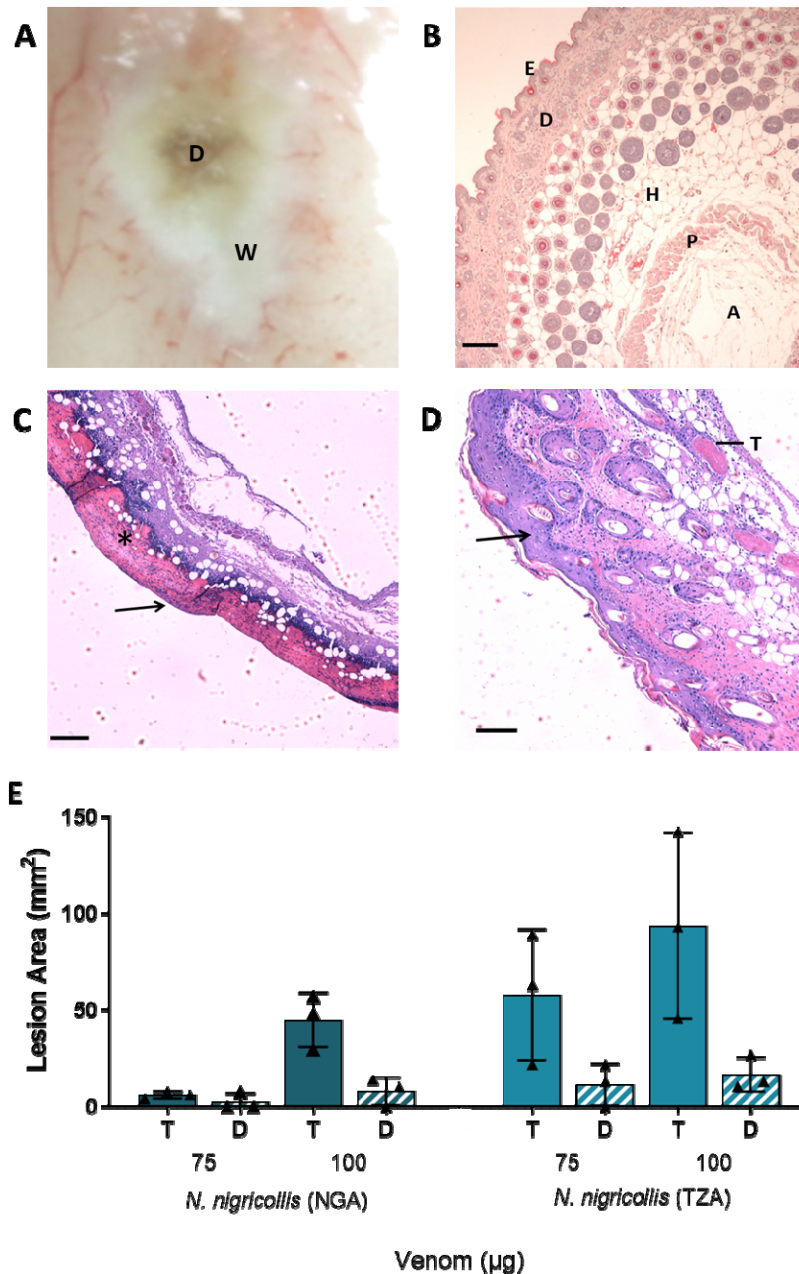


Fig. 1. African spitting cobra venoms cause heterogeneous dermonecrotic lesions *in vivo*. Groups of mice (n=3) were injected intradermally with two doses of spitting cobra venom and after 72 h the resulting lesions were excised for macroscopic quantification of damaged areas and histological assessment. **A)** Representative macroscopic image of a skin lesion induced by 100 µg of venom from West African (Nigeria) *N. nigricollis*, in which a dark central area (D) of necrosis is observed surrounded by a white area (W) of skin damage. **B-D)** Representative light micrographs of sections of the skin of mice injected with PBS or West African *N. nigricollis* venom. **B)** Skin injected with PBS showed a normal histological appearance including the epidermis (E), dermis (D), hypodermis (H), panniculus carnosus (P) and adventitia (A). **C)** Light micrograph of a section of skin corresponding to a dark area of venom-induced damage. All skin layers were affected, with loss of epidermis (arrow) and skin appendages in the dermis. A proteinaceous hyaline material was observed (*). **D)** Light micrograph of a section of the

skin corresponding to a white area of damage from a mouse injected with venom. There was an increase in the thickness of epidermis (hyperplasia; arrow) and inflammatory infiltrate in the dermis. Thrombi (T) were observed in some blood vessels. **E)** The area of dermonecrotic lesions caused by *N. nigricollis* (West African, Nigeria [NGA]; East African, Tanzania [TZA]) venoms at different doses. Bars show the mean area of the total lesions (T) in comparison to the dark central areas (D) of greatest intensity, and error bars represent the standard deviation from the mean. Scale bars in B-D represent 100 μm .

Venom CTx are predominately responsible for cytotoxic effects in cell culture

To identify which toxins in spitting cobra venoms are responsible for causing the dermonecrotic effects observed *in vivo*, we first identified and quantified the cytotoxic potency of venom constituents using cell cytotoxicity methods in immortalised human epidermal keratinocytes (HaCaT cell line). This work was performed using East African (Tanzania) *N. nigricollis* venom, which was separated into its distinct constituents via gel filtration and cation exchange chromatography, followed by further purification using hydrophobic interaction or hydroxyapatite chromatography (**Fig. S1-S9**). The identity of the isolated toxins was confirmed by mass spectrometric analysis (**Table S1**). The HaCaT cells were then exposed to either crude venom, four purified CTx (CTx1, CTx1v, CTx3 and CTx4), or two purified PLA₂ (basic and acidic), and combinations consisting of all CTx (at a ratio reflective of relative abundance in the venom; ~3:1:1:1), all PLA₂ (1:1), and all CTx and PLA₂ together in a 2:1 ratio (reflective of that found in the crude venom (32)). Following venom exposure we performed thiazole blue tetrazolium (MTT) assays to assess cell viability via measures of metabolic activity (33, 34) multiplexed with propidium iodide (PI) assays as an indicator of cell death associated with plasma membrane disruption (35) (**Fig. 2**).

MTT measurements of cell viability, taken after 24 h of treatment, showed that crude venom potently reduced cell viability (IC_{50} 22.9 $\mu\text{g}/\text{mL} \pm 0.7$; **Fig. 2A**). Similarly, all four of the purified venom CTx reduced cell viability, with CTx3 being the most potent (IC_{50} 20.8 $\mu\text{g}/\text{mL} \pm 2.5$), followed by CTx4 (IC_{50} 37.2 $\mu\text{g}/\text{mL} \pm 1.2$), and then CTx1 and CTx1v, which showed similar potencies (IC_{50} 63.4 $\mu\text{g}/\text{mL} \pm 9.0$ and 53.5 $\mu\text{g}/\text{mL} \pm 18.4$, respectively) and were significantly less potent than CTx3 ($P = 0.004$ and $P = 0.020$, respectively; **Fig. 2C, H**). While the basic PLA₂ visibly showed some cell viability inhibitory effects at the highest concentrations tested ($\geq 100 \mu\text{g}/\text{mL}$), neither of the two purified PLA₂ alone (**Fig. 2F**) or combined in a 1:1 ratio (**Fig. 2E**) were sufficiently toxic to the cells to allow for the calculation of IC_{50} values. The combination of the four purified CTx gave a complete concentration-response curve with a resulting IC_{50} value approaching those obtained with crude venom (27.0 $\mu\text{g}/\text{mL} \pm 3.6$ vs 22.9 $\mu\text{g}/\text{mL} \pm 0.7$, respectively; **Fig. 2B**), though remained slightly right-shifted in comparison (**Fig. 2G**). When the CTx and PLA₂ combinations were pooled together in a 2:1 ratio, reflective of their toxin abundance in crude east African *N. nigricollis* venom (32), the resulting concentration-response curve became indiscernible from that of the crude venom and

resulted in a near-identical IC_{50} value ($22.6 \mu\text{g/mL} \pm 1.5$ vs $22.9 \mu\text{g/mL} \pm 0.7$, respectively) (Fig. 2H).

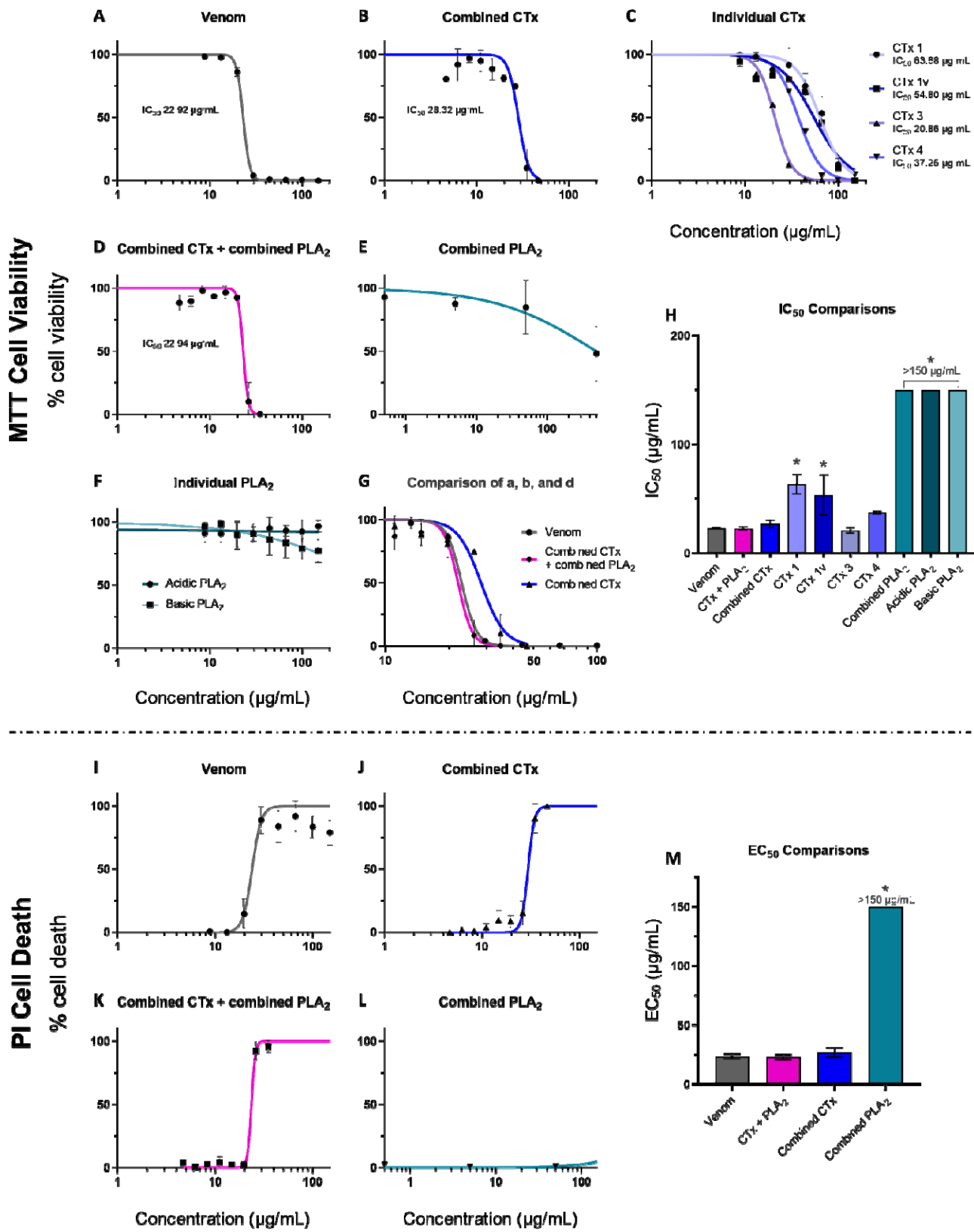


Fig. 2. Crude venom and purified CTx inhibit cell viability, with CTx venom activity modestly potentiated by PLA₂ toxins. Cell viability was measured in immortalised

human keratinocytes (HaCaT cells) using MTT assays (A-H) and multiplexed with propidium iodide (PI) assays to measure cell death (I-M). HaCaT cells were treated for 24 h with serial dilutions of East African (Tanzania) *N. nigricollis* venom or its isolated toxins. MTT concentration-response curves are shown for: **A**) crude east African *N. nigricollis* venom, **B**) combined purified CTx, **C**) individual purified CTx, **D**) combined CTx and combined PLA₂ together, **E**) combined purified PLA₂, and **F**) individual purified PLA₂. **G**) Direct comparison of the concentration-response curves caused by crude venom, combined CTx, and the combined CTx + combined PLA₂ together. Note the different scale on the x-axis in comparison with panels A-F. **H**) IC₅₀ value summary of the various venom toxins displayed in A-F using MTT assays. PI concentration-response curves are shown for: **I**) crude *N. nigricollis* venom, **J**) combined purified CTx, **K**) combined CTx and combined PLA₂ together, and **L**) combined purified PLA₂. **M**) EC₅₀ values of the various venom toxins displayed in I-L using PI assays. For panels A-F, the data shown represent mean % cell viability and corresponding standard deviations. For panels I-L, the data shown represent mean % cell death and corresponding standard deviations. All data displayed are from three independent experiments with each condition conducted in triplicate. Data were normalised to 0-100% between the lowest and highest read values for analysis, then plotted as concentration-response curves using GraphPad Prism 9. For panels H and M, statistically significant differences determined by one-way ANOVAs with Dunnett's multiple comparisons post-hoc tests, are denoted by asterisks: * ($P < 0.05$).

PI measurements of cell death taken 24 h post-treatment with the various toxin combinations and east African *N. nigricollis* venom showed similar patterns (**Fig. 2I-M**). The crude venom displayed potent cytotoxic effects resulting in EC₅₀ values of 23.4 $\mu\text{g/mL} \pm 2.4$, while the PLA₂ combination did not cause sufficient cell death at the highest concentrations tested to calculate an EC₅₀ value (**Fig. 2I, L, M**). The CTx combination resulted in an EC₅₀ value close to that of the crude venom (EC₅₀ of 26.8 $\mu\text{g/mL} \pm 4.1$ vs 23.4 $\mu\text{g/mL} \pm 2.4$, respectively), while the 2:1 ratio of CTx:PLA₂ combinations together modestly decreased the EC₅₀ value (22.8 $\mu\text{g/mL} \pm 2.4$), but to levels highly comparable to those obtained with crude venom (**Fig. 2J, K, M**).

The combination of purified CTx and PLA₂ induces venom-induced dermonecrosis *in vivo*

To understand whether CTx are also predominately responsible for dermonecrotic venom activity *in vivo*, we performed comparative experiments in our murine preclinical model of envenoming (36). The minimum necrotic dose (MND) of East African *N. nigricollis* venom, i.e., the dose that induces a lesion in the skin of 5 mm diameter 72 h after injection (36), was determined to be 63 $\mu\text{g}/\text{mouse}$, and doses of purified CTx, PLA₂, and CTx + PLA₂ that reflect their relative mass contribution to the total crude venom protein were determined (CTx and PLA₂ comprise approximately 60% and 26% by weight of *N. nigricollis* venom, respectively (16, 32, 37-39)). Thus, groups of mice received

intradermal injections of either 63 µg of crude venom, 37.8 µg of the purified CTx combination, 16.4 µg of the purified PLA₂ combination, or 37.8 µg plus 16.4 µg of the purified CTx and the PLA₂ combinations, respectively, combined. After 72 h, animals were euthanised, dermonecrotic lesions excised, measured, photographed and processed for histopathological analysis (images of the resulting dermonecrotic lesions are presented in **Table. S2**).

Mean lesion areas resulting from venom injection were large and varied extensively among the experimental animals ($52.0 \text{ mm}^2 \pm 24.6$) (**Fig. 3A**). Mice receiving the CTx and PLA₂ combinations together (CTx + PLA₂) developed lesions that did not differ significantly in size from those induced by the whole venom ($27.7 \text{ mm}^2 \pm 27.8$; $P > 0.05$), suggesting that these two groups of toxins are collectively responsible for recapitulating the major effects of the crude venom. In contrast with our cytotoxicity data, however, the CTx combination alone resulted in negligible dermonecrosis *in vivo*, with only one of the four experimental animals displaying a visible lesion, and the mean lesion size ($2.1 \text{ mm}^2 \pm 4.1$) being significantly lower than that caused by the crude venom ($P = 0.027$). Again in contrast to the cell data, the PLA₂ toxin combination resulted in three of the four mice developing visible lesions ($8.0 \text{ mm}^2 \pm 9.3$), though the mean lesion size remained more than threefold lower than that observed with the crude venom and the CTx and PLA₂ combination together. The overall severity of the lesions was also assessed using our recently developed, AI-based, dermonecrosis quantification tool, VIDAL, which standardises and quantifies lesion size and intensity to calculate an overall dermonecrosis score in Dermonecrosis Units (DnU) (**Fig. S11**) (40). Quantification by VIDAL largely recapitulated the results above (**Fig. 3B**), confirming that lesion severity caused by crude venom ($120.6 \text{ dermonecrotic units [DnU]} \pm 61.6$) was not significantly different from that of the CTx + PLA₂ combination ($66.3 \text{ DnU} \pm 70.2$), and that lesions caused by the CTx combination resulted in significantly less dermonecrosis ($6.8 \text{ DnU} \pm 13.7$, $P = 0.025$) than the crude venom. Lastly, total dermonecrosis scores (41) were calculated after histopathological assessment of H&E-stained lesion cross-sections for each animal (**Fig. 3C**). These data revealed that mice injected with crude venom showed extensive damage in all layers of the skin (dermonecrosis severity score of 2.6 ± 1.6). The PLA₂ treated mice exhibited the next highest dermonecrosis severity scores (2.0 ± 1.5), followed by those receiving the CTx + PLA₂ combination (0.9 ± 0.8) and then the CTx combination only (0.3 ± 0.3). These latter two groups exhibited dermonecrosis severity scores that were significantly lower than that of the crude venom ($P = 0.0218$ and $P = 0.0091$, respectively). Scoring for individual skin layers can be seen in **Fig. S10**.

The PLA₂ inhibitor varespladib protects against venom-induced dermonecrosis

Since our data demonstrated that venom-induced dermonecrosis relies on the combined effect of CTx and PLA₂ venom toxins working together, we hypothesised that inhibiting just one of these toxin classes could significantly reduce the severity of venom-induced dermonecrosis *in vivo*. To that end, we repeated the experiments described above in the presence of the PLA₂ inhibitor varespladib. Varespladib was originally designed for use in

the treatment of cardiovascular diseases (42-44), but has recently entered phase II clinical trials for snakebite envenoming (45) following demonstration of its ability to prevent PLA₂ toxin-driven systemic envenoming pathologies in animal models (29, 30, 46, 47).

We pre-incubated 19 µg of varespladib (41) with the same venom or purified toxin challenge doses before intradermally co-injecting mice and excising and analysing lesions 72 h later, as described above. The co-injection of varespladib with crude venom caused statistically significant reductions in lesion sizes from 52.0 mm² (± 24.6) to 2.6 mm² (± 5.3) ($P = 0.001$; **Fig. 3D**). Co-injection of varespladib with the CTx + PLA₂ combination also caused a substantial reduction in mean lesion size from 27.7 mm² (± 27.8) to 5.5 mm² (± 6.4), although this reduction was not statistically significant. Unsurprisingly, varespladib did not affect the minor lesion formation observed in the group dosed with the CTx combination, though when varespladib was dosed alongside the purified PLA₂, the resulting lesion sizes decreased from a mean of 8.0 mm² (± 9.3) to no lesions being formed in any of the four experimental animals. These results were confirmed with the AI-generated dermonecrosis severity scores (**Fig. 3E**), from which the crude venom-induced lesions of 120.6 DnU ± 61.6 decreased significantly to 3.6 DnU ± 8.1 ($P=0.0054$) when co-incubated with varespladib. Similar effects of varespladib were seen when varespladib was co-incubated with the CTx + PLA₂ combination (decreasing mean lesion score from 66.3 DnU ± 70.2 to 24.7 DnU ± 30.7) and PLA₂ (decrease from 29.2 DnU ± 36.9 to 5.9 DnU ± 11.8), albeit these were not statistically significant. Decreases in lesion severity were not observed when varespladib was co-treated with CTx. Histopathological analyses of skin lesion cross-sections also correlated with the macroscopic assessment of dermonecrosis. Mice receiving venom pre-incubated with varespladib showed significantly less microscopic damage than those that received venom alone (dermonecrosis severity scores: venom, 2.6 ± 1.6; venom and varespladib, 0.0 ± 0.0; $P = 0.0035$) (**Fig. 3F**). Reductions in microscopic damage by varespladib were also observed in animals receiving either the PLA₂ + CTx combination or PLA₂ dose, although these were not statistically significant (dermonecrosis severity scores: PLA₂ + CTx, 0.9 ± 0.8 vs PLA₂ + CTx and varespladib, 0.3 ± 0.4; PLA₂, 2.0 ± 1.5 vs PLA₂ and varespladib, 0.0 ± 0.0). Full details of the dermonecrosis severity scores obtained across each individual skin layer are presented in **Fig. S10**.

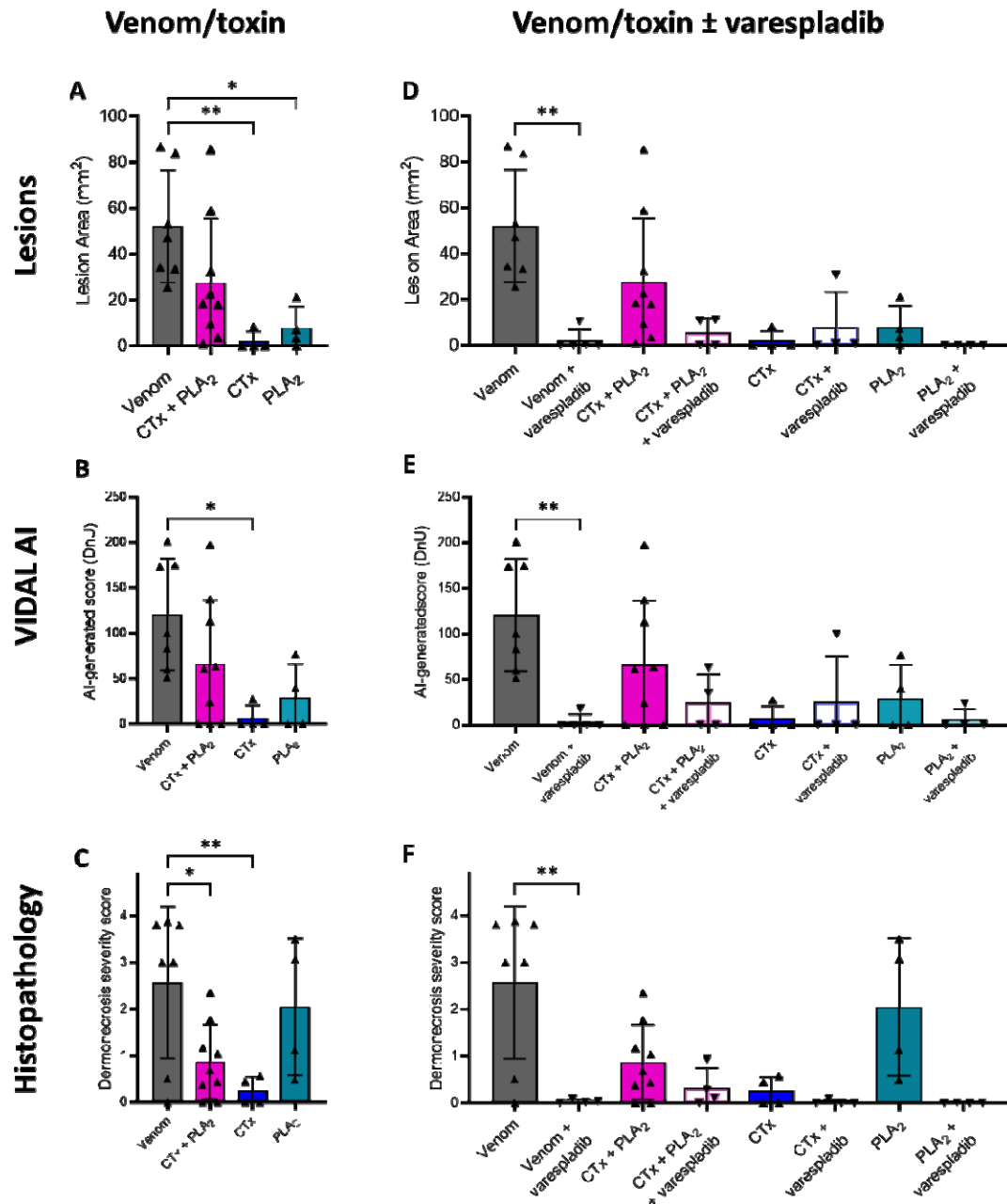


Fig. 3. Spitting cobra venom causes dermonecrosis *in vivo* via CTx and PLA₂ toxin potentiation, and inhibition of PLA₂ toxins with varespladib reduces dermonecrosis severity. Groups of mice (n≥4) were intradermally injected with either East African (Tanzania) *N. nigricollis* venom or purified venom constituents (CTx, PLA₂, or a combination of CTx + PLA₂) at doses reflecting their relative abundance in crude venom, with or without the PLA₂-inhibiting small molecule drug varespladib (19 μg). At 72 h post-injection, lesions were excised and examined macroscopically and histopathologically. **A)** A combination of venom CTx and PLA₂ was required to recapitulate the dermonecrotic activity of crude *N. nigricollis* venom, as CTx and PLA₂ toxins alone did not cause extensive dermonecrosis, as quantified via **A)** calliper-measurements of lesion height and width, and **B)** the lesion severity measuring AI tool, VIDAL. **C)** Histopathological analysis of excised lesions showed similar results, except

for a more severe dermonecrotic effect of the PLA₂ alone. Pre-incubation with the PLA₂ inhibitor varespladib reduced dermonecrotic lesion severity caused by East African *N. nigricollis* venom with similar trends for CTx + PLA₂ and PLA₂, as quantified with **D**) callipers, **E**) VIDAL, and **F**) histopathological analysis. For damage scores of individual skin layers see **Fig. S10**. For panels A and D, the data shown represent mean lesion areas and corresponding standard deviations. Panels B and E show the mean lesion severity, as determined by VIDAL. Panels C and F show mean dermonecrosis severity scores and corresponding standard deviations calculated from those of the individual skin layers (**Fig. S10**). Statistically significant differences were determined by one-way ANOVAs followed by Tukey's multiple comparisons post-hoc tests and are denoted by asterisks: * ($P < 0.05$), ** ($P < 0.01$). Error bars represent standard deviations.

To confirm that the inhibitory effect of varespladib is the sole result of inhibition of PLA₂-driven toxicity, we performed MTT cell cytotoxicity assays, as described previously, using either East African *N. nigricollis* venom or the CTx combination preincubated with and without a cell-tolerated high dose of varespladib (128 μ M) (41). As anticipated, while varespladib significantly reduced the cytotoxicity of crude venom (22.9 μ g/mL \pm 0.7 vs 30.3 μ g/mL \pm 2.0, $P = 0.004$), no significant effect on cell viability was observed when the PLA₂ inhibitor was co-incubated with purified CTx (27.0 μ g/mL \pm 3.6 vs 29.2 μ g/mL \pm 3.8, $P > 0.05$) (**Fig. 4**), thereby confirming that varespladib is only interacting with PLA₂ toxins.

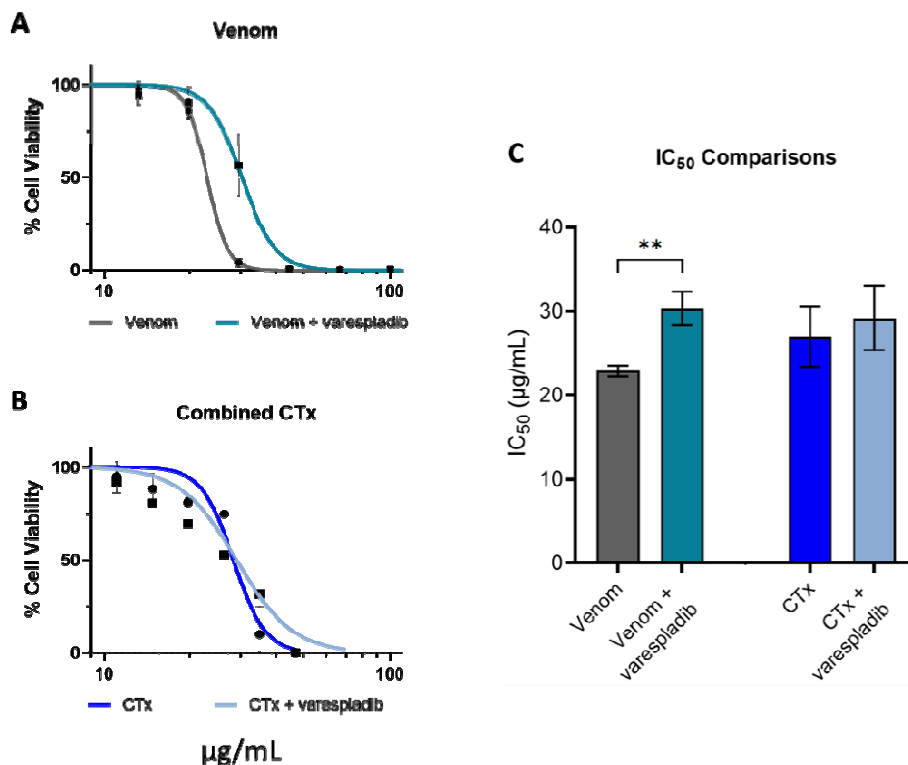


Fig. 4. Preincubation with the PLA₂ inhibitor varespladib has no effect on CTx-induced loss of cell viability in keratinocytes. Cell viability was measured in immortalised human keratinocytes (HaCaT cells) using MTT assays, with cells treated for 24 h with serial dilutions of (A) East African (Tanzania) *N. nigricollis* venom or (B) the purified CTx combination, with or without preincubation with 128 µM varespladib. The data shown represent mean percentage cell viability and corresponding standard deviations, with data normalised to 0-100% between the lowest and highest absorbance values for analysis, then plotted as dose-response curves using GraphPad Prism 9. All data displayed are from three independent experiments with each condition in triplicate. (C) IC₅₀ values of the venom and CTx combination, with and without varespladib, displayed in A and B. The data shown represent the mean IC₅₀ values of curves and corresponding standard deviations. Statistically significant differences were determined by unpaired t-tests and are denoted by asterisks: ** ($P < 0.01$).

To investigate whether the inhibitory effect of varespladib might extend to other cobra species, we next used venom from a related African spitting cobra species, the red spitting cobra *N. pallida*, which diverged from *N. nigricollis* around 6.7 million years ago (21), using the same *in vivo* model of dermonecrosis. Preincubation with varespladib resulted in complete abolition of lesion formation caused by *N. pallida* venom, with no lesions observed in any of the five experimental animals receiving the drug (venom, $32.4 \text{ mm}^2 \pm 18.1$ vs venom and varespladib, $0.0 \text{ mm}^2 \pm 0.0$; $P = 0.0039$) (Fig. 5A); a result that was also confirmed with the lesion severity scores calculated by VIDAL ($59.0 \text{ DnU} \pm 28.2$ versus $0.0 \text{ DnU} \pm 0.0$, respectively; $P = 0.0054$) (Fig. 5B). Images of the resulting dermonecrotic lesions are presented in Table. S3. Further, histopathological assessment of venom-induced skin pathology also resulted in significant decreases in both total dermonecrosis scores (venom, 2.0 ± 1.2 ; venom and varespladib, 0.1 ± 0.1 ; $P = 0.009$) and for several individual skin layers analysed (epidermis, $P = 0.003$; hypodermis, $P = 0.027$; panniculus carnosus, $P = 0.005$) (Fig. 5C and D). Given that spitting cobra venom profiles share high levels of toxin similarity (21, 32), these findings provide confidence in the general effectiveness of varespladib against venom-induced dermonecrosis stimulated by geographically diverse African spitting cobra venoms.

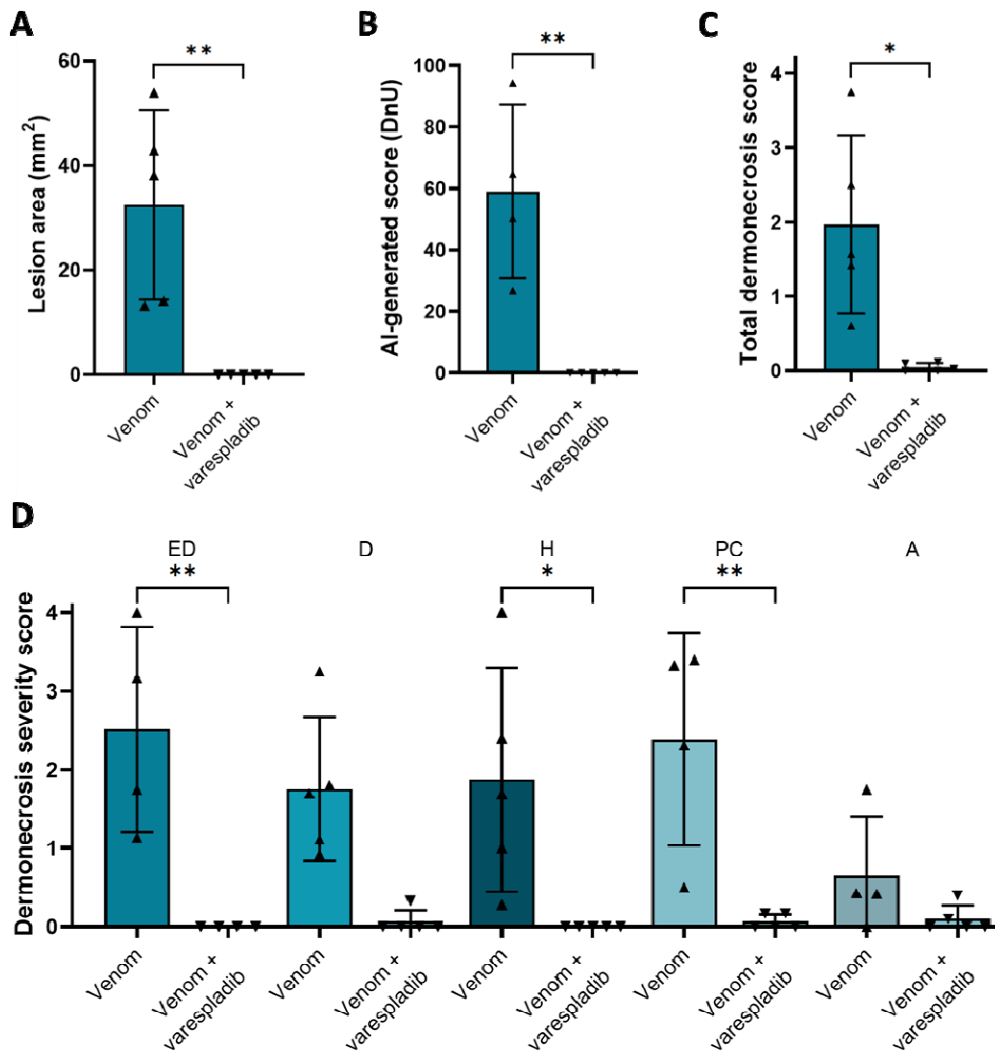


Fig. 5. Dermonecrosis caused by *N. pallida* venom is prevented by the PLA₂ inhibitor varespladib. Groups of mice (n=5) were intradermally injected with 25 μ g *N. pallida* venom with or without the PLA₂ inhibiting drug varespladib (19 μ g). At 72 h post-injection, lesions were excised and examined, from which it was determined that the PLA₂ inhibitor varespladib significantly reduced the size and severity of the dermonecrotic lesions caused by *N. pallida* venom as measured with **A**) callipers, **B**) VIDAL, and **C**) histopathological analysis of the **D**) different skin layers (ED, epidermis; D, dermis; H, hypodermis; PC, panniculus carnosus; A, adventitia). For **C** and **D**, the data shown represent the total mean dermonecrosis score of all layers, versus the mean damage score for each individual skin layer, respectively, and corresponding standard deviations. Statistically significant differences were determined by unpaired t-test comparisons for A, B, and C, and by two-way ANOVA, followed by Dunnett's multiple comparisons tests for D. Statistically significant differences are denoted by asterisks: * = $P < 0.05$, ** = $P < 0.01$. Error bars represent standard deviations.

Varespladib exhibits *in vivo* efficacy against spitting cobra induced dermonecrosis in delayed treatment models

Next, we sought to explore the inhibitory capability of varespladib in more biologically realistic models of snakebite envenoming, where treatment is delivered after venom challenge (48, 49). In addition, to further assess the cross-species and regional efficacy of varespladib we used another venom, this time from West African (Nigerian) *N. nigricollis*.

Dermonecrosis: Intradermal administration of Varespladib: We repeated our previously described pre-incubation experiments and demonstrated again that the intradermal co-administration of venom with varespladib significantly reduced the size of the resulting skin lesions ($42.8 \text{ mm}^2 \pm 6.7$ for venom vs $2.7 \text{ mm}^2 \pm 6.5$ for venom and varespladib; $P < 0.0001$) (**Fig. 6A**). Then, to better understand whether varespladib could prevent dermonecrosis when administered after envenoming has occurred, and thus more accurately mimic a real-world snakebite scenario, we intradermally injected groups of mice with *N. nigricollis* venom (110 μg) followed by a second intradermal injection of varespladib (100 μg) in the same location at either 0, 15 or 60 minutes later. In all instances, we observed a significant reduction in the size of dermonecrotic lesions when varespladib was administered in comparison with the venom-only control (**Fig. 6B**). Reductions were most substantial in the group that received varespladib immediately after venom injection (0 min), where only one of the experimental animals presented with a small lesion 72 h later, resulting in significantly reduced mean lesion areas of $1.6 \text{ mm}^2 (\pm 2.7)$ compared with $34.0 \text{ mm}^2 (\pm 7.7)$ in the venom-only controls ($P < 0.0001$) (**Fig. 6B**). While we observed reduced therapeutic potency with longer time delays between venom challenge and treatment, reductions in lesion sizes remained statistically significant at both 15- and 60-minutes post-venom challenge ($13.6 \text{ mm}^2 \pm 3.5$ and $16.4 \text{ mm}^2 \pm 5.5$, respectively, vs $34.0 \text{ mm}^2 \pm 7.7$ with the venom only control; $P < 0.0001$) (**Fig. 6B**).

Dermonecrosis: Intravenous administration of Varespladib: To closer mimic current treatment of envenoming with antivenom, we next explored whether intravenous, rather than local, injection of varespladib could reduce venom-induced dermonecrosis. To that end, groups of experimental animals received the same intradermal dose of *N. nigricollis* venom (110 μg), followed by an intravenous injection of varespladib (100 μg) at either 0-, 30-, 60- or 120-min post-venom challenge. However, this dose of intravenous varespladib did not provide any reduction in the size of dermonecrotic lesions when compared with the venom-only control for any of the different dosing timepoints, including when varespladib was injected immediately after the venom challenge ($35.3 \text{ mm}^2 \pm 3.6$ for the venom only control vs $30.1\text{-}34.3 \text{ mm}^2$ for the various timepoint varespladib treatment groups) (**Fig. 6C**).

Myotoxicity: Intravenous and intramuscular administration of Varespladib: Given the generally promising therapeutic findings observed when using varespladib against spitting cobra venoms that cause dermonecrosis, our final experiments assessed whether varespladib could also prevent venom-induced myotoxicity – an envenoming pathology also associated with the cytotoxic action of cobra venoms *in vivo* (50-52) and in cultures of myogenic cell lines (16). We induced myotoxicity in our murine envenoming model via

intramuscular (gastrocnemius) venom injection and quantified muscle tissue damage by measuring plasma creatine kinase (CK) (53) activity 3 h later. When West African *N. nigricollis* venom (10 μ g) was co-administered with varespladib (10 μ g (52)), there was a significant reduction in resulting plasma CK levels compared to those obtained from mice receiving venom alone (venom, 5783.50 U/L \pm 2055.86; venom and varespladib, 1969.50 U/L \pm 448.67; $P = 0.01$) (**Fig. 6D**). Following this, we investigated whether the delayed administration of varespladib would retain efficacy against venom-induced myotoxicity, and we explored this via both intramuscular and intravenous delivery of the drug at the increased dose of 100 μ g, matching the route of venom challenge and current antivenom delivery, respectively. Treatment via both dosing routes resulted in significant reductions in venom-induced increases in plasma CK activity, irrespective of whether treatment was delivered immediately after venom challenge or 15 minutes later (54.48-69.59% reduction of plasma CK after varespladib injection vs venom-only control; $P \leq 0.018$ for all comparisons). Unlike that observed with the dermonecrosis experiments, there was little difference in drug efficacy between the two delivery routes tested, with the mean plasma CK activity of mice that received intravenous varespladib marginally lower than in those that received the therapy intramuscularly (2442.75 vs 2797.40, 0 mins; 2398.75 vs 3656.80, 15 mins; intravenous vs intramuscular, respectively), though these differences were not statistically significant (**Fig. 6E**).

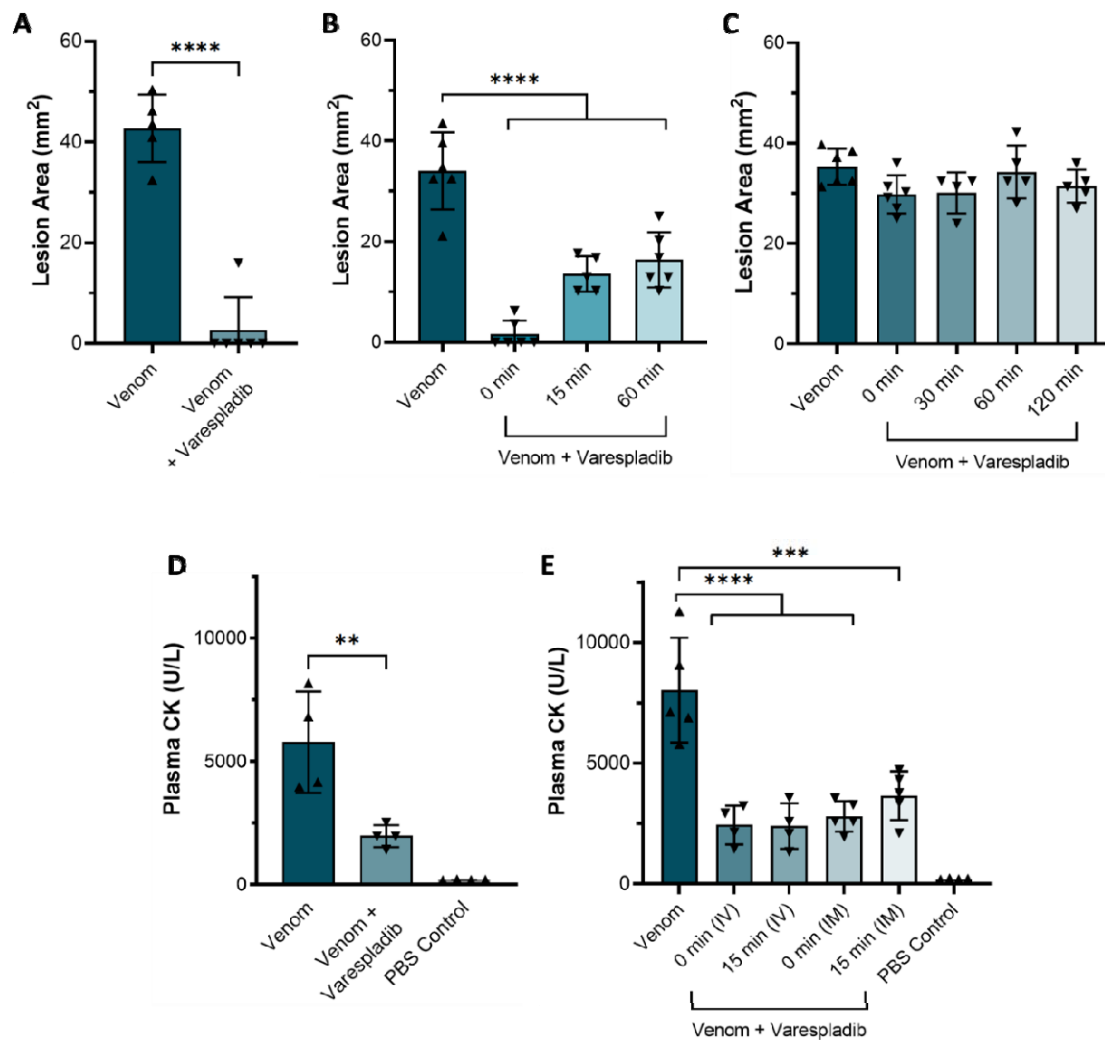


Fig. 6. Delayed administration of varespladib following spitting cobra envenoming causes significant reductions in dermonecrosis and myotoxicity *in vivo*. Groups of mice ($n \geq 4$) were injected with either West African (Nigeria) *N. nigricollis* venom alone or followed by varespladib at a range of different timepoints and via different administration routes. **A**) Intradermal co-administration of preincubated venom (110 μ g) and varespladib (20 μ g) significantly reduced the size of skin lesions caused by west African *N. nigricollis* venom 72 h later. **B**) Intradermal administration of varespladib (100 μ g) 0, 15 and 60 min after intradermal venom challenge (110 μ g) resulted in significant reductions in the size of venom-induced dermonecrotic lesions. **C**) Intravenous delivery of varespladib (100 μ g) at 0, 30, 60, and 120 minutes after intradermal venom challenge (110 μ g) resulted in no protection against venom-induced dermonecrosis. **D**) Intramuscular delivery of varespladib (10 μ g) co-incubated with 10 μ g venom resulted in significant reductions in plasma CK activity induced by *N. nigricollis* venom. **E**) Intravenous (IV) and intramuscular (IM) delivery of varespladib (100 μ g) 0 or 15 min after intramuscular venom challenge (10 μ g) resulted in significant reductions in plasma CK activity induced by *N. nigricollis* venom. For panel A, statistically significant differences were determined by an unpaired t-test; for panels B-D, by one-way ANOVAs followed by Dunnett's

multiple comparisons post-hoc tests. Statistically significant differences are denoted by asterisks: * $P < 0.05$, *** $P < 0.001$, and **** $P < 0.0001$.

Discussion

Snakebite results in 2.5 million envenomings each year (54), yet outdated animal-derived antivenoms remain the only specific treatment available (1). Although these therapeutics are undoubtedly lifesaving interventions, their clinical utility is restricted by a lack of affordability, limited breadth of efficacy across different snake species, high incidences of adverse reactions associated with some products and the necessity for snakebite patients to travel, often for several hours, to a hospital for intravenous antivenom administration (1, 22). Critically, antivenoms remain ineffective against the rapidly developing local pathology of snakebite envenoming, which in severe cases can lead to patients requiring tissue debridement around the bite site or amputation of the affected limb or digit (22). There is therefore an urgent and compelling need for research to develop new therapies against local envenoming by African and Asian cobra bites (*Naja* spp.), particularly African spitting cobras (6, 55, 56). Consequently, in this study we sought to: (i) characterise the dermonecrosis caused by the venoms of African spitting cobras, (ii) identify which are the primary aetiological dermonecrosis toxins found within these venoms and (iii) determine whether spitting cobra venom-induced dermonecrosis can be inhibited with the PLA₂-inhibiting drug varespladib.

Using venoms from *N. nigricollis* (east and west African), we first characterised dermonecrotic pathology in a murine model of local envenoming. The results of these studies confirmed a dose-dependent relationship between the amount of venom injected and lesion severity, that the dermal lesions caused by spitting cobra venoms *in vivo* often contain a dark inner region surrounded by a lighter region of skin damage, and that these dark regions show more prominent microscopic damage than the lighter regions. Studies on dermonecrosis induced by cobra venoms, and their inhibition, should therefore consider this dichotomy in the assessment of the pathological effects of their venoms (40).

To elucidate the toxins responsible for inducing dermonecrosis we first used cell cytotoxicity assays with human epidermal keratinocytes as our model, from which we demonstrated that the CTx in east African *N. nigricollis* venom are the toxins predominately responsible for *in vitro* cytotoxicity. Despite PLA₂ having been described as having cytotoxic effects on different cell types (18, 57), the two types of PLA₂ isolated from *N. nigricollis* venom had little effect on keratinocytes in isolation or when combined, though the basic PLA₂ appeared to be slightly more cytotoxic at high concentrations than the acidic PLA₂. Crucially, the combination of purified CTx did not completely replicate the cytotoxic potency of whole venom, which instead required using both the CTx and PLA₂ combinations together (**Fig. 2G**), suggesting that PLA₂ toxins at least mildly potentiate the cytotoxic activity of the CTx in cell culture experiments. This probable synergy between CTx and PLA₂ has been documented in several previous studies that explored the venom of *Naja* and related elapid snake species (19, 21, 58-61); therefore,

these findings are largely consistent with the literature, although the relative contribution of CTx versus PLA₂-mediated cytotoxicity observed here is perhaps surprisingly skewed heavily towards CTx.

The likely synergy between the two toxin families became more apparent *in vivo* (**Fig. 3A-C**), where both CTx and PLA₂ in isolation were found to only cause negligible dermonecrosis in mice, while their combination resulted in extensive dermonecrotic lesions approaching the size and severity of those formed by crude venom, notwithstanding wide inter-animal variability. Further, the CTx only caused modest damage to a single skin layer, the panniculus carnosus, in agreement with the known *in vivo* myotoxic effect of cytotoxic 3FTxs (51). Comparatively, venom and the CTx and PLA₂ combinations together affected all skin layers, which is to be expected based on the large lesions formed by both *in vivo* (**Fig. S10**). These findings indicate that the CTx, which were predominately responsible for cytotoxicity in cell culture (**Fig. 2**), are not directly responsible for necrosis of the dermis and loss of the epidermis caused by spitting cobra venom *in vivo* (62). Interestingly, histopathologically determined dermonecrosis severity scores in PLA₂-induced lesions were high, despite the small lesion size. This may suggest that PLA₂ toxins can cause severe dermonecrosis focally, but without the presence of CTx this damage is limited in extent.

This necessity for both CTx and PLA₂ toxins to be injected concurrently to cause extensive dermonecrosis is a notable finding, and directly correlates with recent data demonstrating that spitting cobra PLA₂ toxins have evolved to potentiate the algescic effect of CTx to cause enhanced pain during defensive venom spitting (21). This means that spitting cobra dermonecrosis, and thus morbidity observed in snakebite victims, may be a direct consequence of the defensive origin of cobra venom spitting. In the context of snakebite therapeutics, our findings evidencing that a combination of CTx and PLA₂ are required to cause dermonecrosis *in vivo* are notable, because they suggest that inhibiting either one of these toxin families could significantly reduce the overall pathology caused by the venom.

Varespladib inhibits PLA₂ from a range of snake venoms, including non-spitting cobras, such as *N. naja*, *N. atra*, and *N. kaouthia* (30), other elapids (31, 63) and several viperids (30, 31). Consequently, varespladib has been selected as a lead candidate as a new snakebite drug, and is currently undergoing clinical development for snakebite (45). However, research associated with varespladib has primarily focused on its potential utility in preventing or delaying the onset of systemic envenoming (45, 46). It has not, until now, been explored in the context of local necrosis following spitting cobra envenoming. Our *in vivo* preclinical efficacy experiments demonstrate that varespladib holds much therapeutic promise for this indication, as co-treatment with varespladib significantly inhibited the formation of dermal lesions caused by east and west African *N. nigricollis* and *N. pallida* venoms (**Fig. 3, 5, and 6**). We found no evidence that varespladib inhibits the activity of CTx (**Fig. 3 and 4**), and thus these data support our hypothesis that a single drug targeting one toxin family (PLA₂) can significantly reduce the severity of local envenoming caused by cobra venom. This is particularly noteworthy

when considering that *Naja* venoms typically contain more CTx than PLA₂, often twice as much based on venom weight, and that spitting cobra venoms share a relatively high degree of compositional similarity to one another (12, 21, 32, 64) particularly in the wider context of inter-specific venom variation (12, 65). Given that varespladib previously entered Phase III clinical trials for other indications (66), and that its oral prodrug form varespladib-methyl is currently in Phase II clinical trials for snakebite in the USA and India (45), our findings suggest that repurposing this drug as a broad-spectrum treatment for preventing spitting cobra-induced dermonecrosis as well, which causes extensive morbidity in sub-Saharan Africa, could be a valuable future application.

Despite these exciting findings, it was important to address the limitations with the animal model of venom-induced dermonecrosis described above (49), where venom challenge and treatment are preincubated and co-administered in a manner artificial to real-world treatment of snakebite envenoming. Consequently, we assessed whether the observed efficacy of varespladib held when used as a treatment after venom challenge, for which we used west African *N. nigricollis* venom (**Fig. 6**). Independent intradermal injection of varespladib at the same site of the venom challenge resulted in significant reductions in the resulting venom-induced lesion sizes, even when treatment was delayed until 60 minutes after envenoming, and treatment with varespladib immediately after venom challenge resulted in comparable efficacy to when the drug was co-administered in the preincubation model (**Fig. 6A, B**). Together, these data suggest that varespladib introduced directly into the tissue where a victim was bitten could significantly reduce the resulting dermonecrosis, particularly if administered soon after a bite. Transdermal drug delivery systems are well-established approaches that could be readily applied here to achieve rapid delivery of varespladib to snakebite victims in a community setting (67, 68). Such an approach has the potential to drastically reduce the time between bite to initial treatment from hours or days (25, 26, 69) to minutes, thus drastically improving the prognosis of tropical snakebite victims.

Since varespladib administered intravenously proved ineffective against venom-induced dermonecrosis (**Fig. 6C**), these findings suggest that an intravenous, and therefore also an oral, version of the drug is less likely to be effective at preventing dermonecrosis. However, these data may simply reflect that, at the dose tested, insufficient varespladib is able to rapidly penetrate from the circulation into the affected peripheral tissue to prevent venom toxicity. Additionally, perhaps a different venom-inhibiting molecule with superior tissue-penetrating properties to varespladib would prove more effective in such experiments. Pharmacokinetic (PK) experiments are therefore required to robustly explore whether intravenous or oral delivery of PK-optimised doses of varespladib, or other inhibitors, might also be effective routes of delivery for the treatment of severe local dermonecrosis.

The myonecrosis-reducing effects of both intramuscular and intravenous injected varespladib (**Fig 6E**) suggests that both local and central methods of administration could be effective at preventing muscle toxicity associated with cobra snakebites. We hypothesise this difference in efficacy between myo- and dermo-necrosis rescue is due to

the comparatively greater abundance of blood vessels in muscle versus cutaneous tissue, resulting in a greater and more rapid distribution of varespladib to the former (70, 71).

Despite the promising results of this study, there are several limitations. Firstly, the variation between the results of our *in vitro* and *in vivo* assays demonstrates that the action of spitting cobra venoms or toxins on keratinocytes does not replicate the complex pathological effects caused in skin *in vivo*. This highlights the need for further research into developing more accurate *in vitro* models of dermonecrosis, perhaps with organoids, organotypics and/or *ex vivo* skin models seeming likely to be valuable tools for future research (72). Additionally, murine models can only act as a guide for the effect a treatment may have in human patients (73), given differences between human and murine metabolism and immune systems (74), as well as differences in skin thickness and structure (75). Further, clinical trials will be needed to fully gauge the effect of varespladib against the local tissue-damaging effects of spitting cobra venoms in humans. Finally, our data was entirely focused on African spitting cobra venoms. Similar experiments should be performed using the venoms of cobra species from additional localities, particularly those found in Asia, to better determine the pan-cobra potential of varespladib as a novel treatment for local envenoming.

In summary, our study has shown that CTx found in spitting cobra venom are largely responsible for causing venom cytotoxicity in cellular assays, but that both CTx and PLA₂ together are required to fully recapitulate the dermonecrotic effects of crude venom *in vivo*. Consequently, a drug that inhibits just one of these toxin types is likely to significantly reduce the overall dermonecrosis caused by crude venom. We tested this hypothesis using the repurposed PLA₂-inhibiting drug varespladib and demonstrated impressive preclinical efficacy of the drug against three geographically diverse African spitting cobra venoms. Most notably, the local injection of varespladib was able to significantly reduce the extent of dermonecrosis, even when dosed up to an hour after venom challenge, and protection conferred by the drug also extended to venom-induced myotoxicity. Collectively, our data suggest that varespladib could become an invaluable new treatment against the tissue-damaging effects of spitting cobra venoms, which cause extensive morbidity in snakebite victims across the African continent.

Materials and Methods

Chemicals, Drugs and Biological Materials

Thiazolyl blue methyltetrazolium bromide (MTT; M5655), dimethyl sulfoxide (DMSO; 276855), propidium iodide (PI; P4170), and varespladib (SML1100; stock solution of 65.7 mM [25 mg/mL] in DMSO) were purchased from Sigma-Aldrich (Merck). Varespladib used in delayed treatment *in vivo* experiments was provided by Dr. Matthew Lewin (Ophirex Inc., Corte Madera, CA, USA). Dulbecco's modified Eagle's medium (DMEM; 11574516), foetal bovine serum (FBS; 11573397), FluoroBrite DMEM (A1896701), glutaMAX supplement (35050038), penicillin-streptomycin (11528876), phosphate

buffered saline (11503387), and TrypLE Express were purchased from Gibco (Thermo Fisher Scientific).

Venoms

Venoms were sourced from snake specimens maintained in the Liverpool School of Tropical Medicine's (LSTM) Herpetarium. This facility and its snake husbandry protocols are approved and inspected by the UK Home Office and the LSTM Animal Welfare and Ethical Review Boards. Venom pools were from wild-caught animals of differing geographical origins, namely: *Naja nigricollis* (Tanzania and Nigeria), and *N. pallida* (Tanzania). Crude venoms were lyophilised and stored at 4 °C to ensure long-term stability, then resuspended in PBS (10 mg/mL) and kept at -80 °C until used in the described experiments, with freeze-thaw cycles kept to a minimum to prevent degradation.

Toxin isolation

The initial step in toxin isolation was a large-scale size separation on a gel filtration chromatography column; this separates the 3FTx and PLA₂ toxins from the higher molecular weight proteins (i.e. snake venom metalloproteinases, L-amino acid oxidase and cysteine rich secretory proteins). For this, 100 mg of *N. nigricollis* (Tanzania) venom was dissolved in 5 mL ice-cold PBS (25 mM sodium phosphate pH 7.2, 0.15 M NaCl) and centrifuged at 10,000 xg for 10 minutes. The supernatant was immediately loaded onto a 480 mL column (2.6 x 95 cm) of Superdex 200HR equilibrated in PBS. The column was operated at a flow rate of 1.0 mL/min during loading and 2.0 mL/min for elution. 10 mL fractions were collected after the void volume and elution was monitored at 280 nm (see **Fig. S1**). SDS-PAGE analysis was carried out on all fractions seen to contain protein on the trace. PLA₂ and 3FTx, respectively, were found to be wholly contained in overlapping peaks 1 and 2. Since their separation was incomplete at this stage, these peaks were pooled in preparation for a second step on cation exchange chromatography. This PLA₂/3FTx pool was dialysed against 50 mM sodium phosphate, pH 6.0 and then applied to a 20 mL HPSP HiPrep column equilibrated in the same buffer. Elution was carried out using a 15-column volume (CV) gradient of 0 - 0.7 M NaCl in 50 mM sodium phosphate, pH 6.0. The flow rate was 1.5 mL/min. The unbound material was retained and 10 mL fractions collected from the start of the NaCl gradient. Elution was monitored at 280 nm (**Fig. S2**). SDS-PAGE analysis was carried out on the main peaks (**Fig. S3**). Cation exchange peaks 3, 4, and 11 contained a band at 14 kDa, assumed to be PLA₂ and based on the relative elution position, 3, 4 are acidic PLA₂ and 11 is basic PLA₂. Peaks 5-9 each contained equal-sized bands that ran just below the 10 kDa marker, characteristic of 3FTx proteins. The major 3FTx fractions, peaks 6, 8, and 9, were pooled back together and dialysed against PBS to form the whole 3FTx fraction, containing the major 3FTx cytotoxins 1, 3 and 4 [see below], used for the *in vivo* studies, and referred to as CTx in this study.

Purification of acidic PLA₂. As judged by SDS-PAGE and RP-HPLC (see **Fig. S8**), the PLA₂ in peak 4 was sufficiently pure for cytotoxicity studies. It was found to have a mass of 13,287 Da. MS/MS of tryptic peptides (see methods below) matched this protein to acidic phospholipase A2 CM-I P00602 from *N. mossambica* (see **Table S1**). The PLA₂ in

peak 3 required a third chromatography step for full purity. This fraction was loaded directly onto a 4.7 mL column of Phenyl Sepharose LS FF equilibrated in 25 mM sodium phosphate pH 7.2. Elution was carried out with a 0-100% (4 CV) gradient of 25 mM sodium phosphate pH 7.2 to 25% ethanol in 25 mM sodium phosphate pH 7.2 with long hold step (5 CV) in the latter buffer. The column was operated at 1.0 mL/min and elution was monitored at 214 nm (see **Fig. S4**). The mass of the purified protein, eluting between 30 and 40 minutes, was found to be 13,172 Da and it was also matched to acidic phospholipase A2 CM-I P00602 ('acidic PLA₂') from *N. mossambica* following trypsin digestion and MS/MS (see **Table S1**). The two acidic PLA₂ forms were combined and used as a single acidic PLA₂ pool throughout the study.

Purification of basic PLA₂. Peak 11 from the cation exchange chromatography step was dialysed against 5 mM sodium phosphate pH 6.8 and then loaded onto a 1 mL column of ceramic hydroxyapatite (CHT I, BioRad) equilibrated in the same buffer. Using a flow rate of 0.5 mL/min, elution was carried out with gradient of 5 mM sodium phosphate pH 6.8 to 500 mM sodium phosphate pH 6.8, 0.15 M NaCl over 20 CV. Elution was monitored at 214 nm (see **Fig. S5**). The protein in the main peak (eluting between 35 and 40 mins) was pure as determined by SDS-PAGE and RP-HPLC (see **Fig. S8**), and was found to have a mass of 13,249 Da. Trypsin digestion with MS/MS analysis resulted in a match to Phospholipase A2 'basic' P00605 ('basic PLA₂') from *N. nigricollis* (see **Table S1**).

The basic PLA₂ and the two acidic PLA₂ were pooled back together and dialysed against PBS to form the combined PLA₂ fraction used in the *in vivo* studies.

Purification of individual 3FTx cytotoxins for cell cytotoxicity studies. The material in peak 6 from cation exchange chromatography was fairly pure as determined by RP-HPLC, but it was highly purified using hydrophobic interaction chromatography (HIC). For this, the fraction was made up to 1.5 M in NaCl and loaded onto a 10 mL Phenyl Superose column. Proteins were then eluted in a 5 CV gradient of 1.5 M NaCl in 25 mM sodium phosphate pH 7.2 to 30% (v/v) ethylene glycol in 25 mM sodium phosphate pH 7.2. The flow rate was 1 mL/min and elution was monitored at 214 nm (see **Fig. S6**). The protein in the main peak (eluting at 50 mins) was found to be pure by SDS-PAGE and RP-HPLC and its mass was determined to be 6,817 Da. MS/MS of tryptic peptides confirmed this protein to be Cytotoxin 1 P01468, referred to as CTx1 throughout this study.

RP-HPLC analysis showed that peaks 8 and 9 together contained three main 3FTx forms. These were separated using HIC as for peak 6. The conditions were identical, except that the starting buffer was 1.2 M NaCl rather than 1.5 M. As can be seen in **Fig. S7**, the three proteins are fully separated by these means. RP-HPLC analysis showed each of these to be pure (**Fig. S9**) and to possess very characteristic peak shapes. All three were subjected to digestion with trypsin and identified using MS/MS. Peak 12 had a mass of 6,707 Da and was identified to be Cytotoxin 4 P01452 (CTx4 in this study). Peak 13 had a mass of 6,817 Da and was identified using MS/MS to be Cytotoxin 1 P01468. This is likely to be a version of the protein identified in peak 6 with a Asn/Asp modification and is named

hereafter as CTx1v. Peak 14 had a mass of 6,884 Da and was determined to be Naniproin/Cytotoxin 3 P0DSN1 (CTx3).

Purity analysis methods. SDS-PAGE was carried out using 4-20% acrylamide gels (BioRad) and run using a Tris-glycine buffer system, followed by staining with Coomassie Blue R250. RP-HPLC was performed on a Vanquish HPLC system (Thermo) using a Biobasic C4 column (2.1 x 150 mm). The flow rate was 0.2 mL/min and proteins were separated in a gradient of acetonitrile (see **Fig. S8** and **S9** for gradient formats) in 0.1% trifluoroacetic acid, with monitoring at 214 nm. Between 2-5 µg protein was typically loaded per analysis.

Trypsin digestion and MS/MS analysis. In preparation for analysis, the relevant proteins were desalted on a RP-HPLC column, as above. These were then dried in a centrifugal evaporator, 20 µL H₂O was added and then re-dried. The proteins were then resuspended in 8 M urea/0.1 M Tris-Cl (pH 8.5), reduced with 5 mM TCEP (tris (2-carboxyethyl) phosphine) for 20 min and alkylated with 50 mM 2-chloroacetamide for 15 min in the dark at room temperature. Samples were diluted 4-fold with 100 mM Tris-Cl (pH 8.5) and digested with trypsin at an enzyme/substrate ratio of 1:20 overnight at 37°C. The reaction was terminated by addition of formic acid (FA), and digested peptides were loaded on to Evotips and analysed directly using an Evosep One liquid chromatography system (Evosep Biosystems, Denmark) coupled with timsTOF SCP-mass spectrometer (Bruker, Germany). Peptides were separated on a 75 µm i.d. × 15 cm separation column packed with 1.9 µm C18 beads (Evosep Biosystems, Denmark) and over a predetermined 44-minute gradient. Buffer A was 0.1% FA in water and buffer B was 0.1% FA in acetonitrile. Instrument control and data acquisition were performed using Compass Hystar (version 6.0) with the timsTOF SCP operating in data-dependent acquisition mode.

Fragmentation spectra were searched against an in-house venom gland-derived protein sequence database using Mascot (21, 76). Reverse decoys and contaminants were included in the search database. Cysteine carbamidomethylation was selected as a fixed modification, and oxidation of methionine was selected as a variable modification. The precursor-ion mass tolerance and fragment-ion mass tolerance were set at 10 ppm and 0.04 Da, respectively, and up to two missed tryptic cleavages were allowed. Mascot files were parsed into Scaffold (version 5.0.1, Proteome Software, Inc.) for validation at a protein-level false discovery rate (FDR) of <1%.

Cells

The immortalised human epidermal keratinocyte line, HaCaT (77, 78), was purchased from Caltag Medsystems (Buckingham, UK). Cells were cultured in phenol red-containing DMEM with GlutaMAX supplemented with 10% FBS, 100 IU/mL penicillin, 250 µg/mL streptomycin, and 2 mM sodium pyruvate (standard medium; Gibco), per Caltag's HaCaT protocol. For cell assays that contained the fluorescent dye PI, a medium formulated for fluorescence-based cell assays was used: FluoroBrite DMEM supplemented with 1% GlutaMAX 100x supplement, 1% FBS, 100 IU/mL penicillin, 250 µg/mL streptomycin, and 2 mM sodium pyruvate (minimally fluorescent medium; Gibco).

The cells were split and growth medium changed 2x per week up to a maximum of 30 passages. Cells were maintained in a humidified, 95% air/5% CO₂ atmosphere at 37 °C (standard conditions).

Multiplexed MTT Cell Viability and PI Cell Death Assays

The MTT cell viability (34) and PI cell death assays were completed as described previously (41), with minor modifications. Briefly, HaCaT cells were seeded at 20,000 cells/well in black-sided/clear-bottomed 96-well plates in standard medium and incubated overnight in standard conditions. The following day, standard medium was aspirated and replaced with treatment solutions prepared in minimally fluorescent medium supplemented with 50 µg/mL PI: wells were treated in triplicate with 100 µL of crude venom (9.09-150.00 µg/mL), individual purified CTx (9.09-150.00 µg/mL), individual purified PLA₂ (9.09-150.00 µg/mL), pooled purified CTx (5.96-44.67 µg/mL), pooled purified PLA₂ (0.0005-500 µg/mL), or pooled purified CTx + PLA₂ in a 2:1 ratio (4.68-35 µg/mL) sourced from east African (Tanzanian) *N. nigricollis* venom, then placed back in standard conditions for a further 24 hours. PI fluorescent readings (EX₅₄₄/EM₆₁₂) were collected on a CLARIOstar Plus (BMG Labtech). The treatment solutions were then aspirated and replaced with MTT-containing minimally fluorescent medium (120 µL at 0.83 mg/mL), and the plates incubated for 45 min in standard conditions. Thereafter, the MTT-containing medium was aspirated, 100 µL DMSO added to each well to dissolve the formazan crystals, and absorbance (550 nm) was read for all wells on the CLARIOstar. Experiments were repeated independently on three occasions for each venom or toxin. Subsequently data were normalised to 0-100% between the lowest and highest absorbance values for analysis to represent %-cell death (PI) or %-cell viability (MTT), then plotted as dose-response curves using GraphPad Prism 9. IC₅₀ (MTT) and EC₅₀ (PI) values were calculated using the '[Inhibitor] vs. normalized response -- Variable slope' and '[Agonist] vs. normalized response -- Variable slope' functions, respectively.

Animal ethics and maintenance

Animal experiment protocols were performed using approvals from the Animal Welfare and Ethical Review Boards of the Liverpool School of Tropical Medicine and the University of Liverpool, with licensed approval (PPL# P58464F90) from the UK Home Office, and in accordance with the UK Animal (Scientific Procedures) Act 1986, and the Institutional Committee for the Care and Use of Laboratory Animals (CICUA) of the University of Costa Rica (approval number CICUA 82-2). Male SWISS (CD1) mice (18-27 g; Charles River, Janvier, Animal Facility of Instituto Clodomiro Picado, Costa Rica) were housed in groups of five and acclimated for one week prior to experimentation. Mice used in experiments conducted in Liverpool (**Fig. 3-5**) were given *ad libitum* access to CRM irradiated food (Special Diet Services, UK) and reverse osmosis water in an automatic water system and kept under room conditions of approximately 22 °C, 40–50% humidity, with 12/12-hour light cycles. Mice used in experiments conducted in Costa Rica (**Fig. 1, 6**) were maintained under conditions of 22-24 °C and 60-65% humidity, with 12/12-hour light cycles, and given *ad libitum* access to food and water.

***In vivo* dermonecrosis and co-treatment with varespladib using a preincubation model of envenoming**

For initial experiments (**Fig. 1**) groups of mice (18-20 g; n=3) received intradermal injections in the ventral abdominal region of either 75 µg or 100 µg of the venoms of west African (Nigeria) or east African (Tanzania) *N. nigricollis*, dissolved in 50 µL of PBS; control mice were injected with 50 µL of PBS alone. After 72 h, mice were sacrificed by CO₂ inhalation, the skins were removed, and the areas of the lesions on the inner side of the skin were measured. Then, skin samples were added to 3.7% formalin fixative solution and processed for embedding in paraffin. Sections (4 µm) were collected and stained with haematoxylin-eosin for microscopic assessment. To identify the toxins responsible for causing dermonecrosis and to assess whether varespladib inhibited this effect (**Figs. 3-5, 6A**), groups of mice (n=4-8) were briefly anaesthetised using inhalational isoflurane and then ID-injected in the rear flank with a 50 µL solution of either: (i) east African *N. nigricollis* venom (63 µg), (ii) corresponding proportional amounts of venom CTx (37.8 µg) or PLA₂ (16.4 µg) isolated from the crude venom, (iii) these purified CTx and PLA₂ combined in a 2:1 ratio, reflecting their relative abundance in crude venom (37.8 µg and 16.4 µg, respectively)(16, 32, 38), (iv) *N. pallida* (Tanzania) venom (25 µg), or (v) west African *N. nigricollis* venom (110 µg), all diluted in PBS (pH 7.4). The same experimental design was used for the varespladib-inhibition experiments except that every venom challenge dose was co-incubated with 19 µg of varespladib (41) (**Figs. 3-5**) or 20 µg of varespladib (**Fig. 6A**) (diluted in 98.48% pH 7.4 PBS and 1.52% DMSO) for 30 minutes at 37 °C and then kept on ice until shortly before intradermal injection. Following dosing, all experimental animals were observed frequently to ensure that no signs of systemic envenoming presented (e.g., neuromuscular paralysis), and the development of local lesions were monitored for 72 hrs. Thereafter, experimental animals were humanely euthanised via inhalational CO₂, and the skins around the injection site dissected. The height and width of the lesions on the inner side of the skin were measured in two directions with digital calipers, placed on A4 printout sheets to standardise the AI-lesion analyser which are available in Jenkins, *et al.* (79), and photographed using a Sony DSC-W800 camera. Excised lesions were cut into cross-sections down the centre of the lesions, placed in plastic tissue cassettes (Sigma-Aldrich [Merck]; Z672122) and fixed in 3.7% formalin pots (CellPath; 13191184) for a maximum of 72 h prior to preparation for downstream histopathology.

Delayed treatment models of *in vivo* dermonecrosis with varespladib

To assess inhibition of dermonecrosis (**Fig. 6**), groups of mice (n=4-6; 22-24 g) received an intradermal injection of 110 µg west African (Nigeria) *N. nigricollis* venom dissolved in 50 µL PBS. Then, at various time intervals after venom (either immediately [0 min], 15 min, or 60 min), a solution of varespladib (100 µg dissolved in 50 µL PBS) was injected intradermally at the same site of venom injection. In the case of venom only controls, 50 µL of PBS was administered intradermally at the site of venom injection immediately after venom. Similar experiments were then performed using intravenous delivery of varespladib. After the intradermal injection of 110 µg *N. nigricollis* venom, varespladib (100 µg in 50 µL PBS) was administered intravenously in the caudal vein, either

immediately (0 min), or 30, 60 or 120 min after venom. Control groups of mice received 110 µg of venom and PBS intravenously instead of varespladib. At 72 h, mice were sacrificed by CO₂ inhalation, the skin was removed and the areas of the necrotic lesions in the inner side of the skin were measured as previously described.

***In vivo* models of myotoxicity and treatment with varespladib**

To assess inhibition of myotoxicity (**Fig. 6**), west African (Nigeria) *N. nigricollis* venom was incubated with varespladib at 37 °C for 30 minutes. Then, aliquots of 50 µL, each containing 10 µg venom and 10 µg varespladib, were injected intramuscularly into the right gastrocnemius muscle of groups of mice (n=4-5; 18-20 g). Controls included mice receiving 10 µg of venom alone and mice receiving 50 µL PBS alone. Three hours after venom injection, blood samples were collected into heparinised capillary tubes under light inhaled isoflurane anaesthesia by cutting the tip of the tail. After centrifugation, the CK activity of plasma was quantified by using a commercial kit (CK-NAC-UVAA kit; Wiener Laboratories, Rosario, Argentina). CK activity was expressed as units/litre (U/L). Additionally, experiments in which varespladib was administered after venom injection were performed (**Fig. 6**). For this, mice received an intramuscular injection, in the right gastrocnemius, of 10 µg west African (Nigeria) *N. nigricollis* venom, dissolved in 50 µL PBS. At various time intervals after venom injection (either immediately [0 min], or at 15 min), a dose of 100 µg varespladib, dissolved in 50 µL PBS, was administered either intramuscularly at the site of venom injection, or intravenously in the caudal vein. A control group of mice received 10 µg venom intramuscularly and PBS by either route instead of varespladib immediately after venom injection. Another control group received only 50 µL PBS by the intramuscular route.

Lesion severity scoring using the Venom Induced Dermonecrosis Analysis tool: VIDAL

The severity of the dermonecrotic lesions was assessed using our newly developed AI analyser, VIDAL, the details of which can be found in Laprade, *et al* (40). Briefly, images of the dissected lesions on A4 standardisation cut out masks (79) were uploaded to the AI's website (<https://github.com/laprade117/VIDAL-Experiments>). The program measured and scored the dark and light regions of the lesions from which it calculated a total dermonecrosis score, given the appropriately named Dermonecrotic Units (DnU), where the higher the number the more severe the lesion.

Histopathological analysis of excised tissue samples

Formalin-stored tissue samples were processed using a Tissue-Tek VIP (vacuum infiltration processor) overnight, before being embedded in paraffin (Ultraplast premium embedding medium, Solmedia, WAX060). Four micrometer paraffin sections were cut on a Leica RM2125 RT microtome, floated on a water bath, and placed on colour slides (Solmedia, MSS54511YW) or poly-lysine slides (Solmedia MSS61012S) to dry. For haematoxylin & eosin (H&E) staining, slides were dewaxed in xylene and rehydrated through descending grades of ethanol (100%, 96%, 85%, 70%) to distilled water before being stained in haematoxylin (5 mins), “blued” in tap water (5 mins) and stained in eosin

(2 mins). Slides were then dehydrated through 96% and 100% ethanol to xylene and cover slipped using DPX (CellPath SEA-1304-00A). Haematoxylin (Atom Scientific, RRBD61-X) and eosin (TCS, HS250) solutions were created in house. Brightfield images of the H&E-stained lesions were captured with an Echo Revolve microscope (Settings: 10x magnification; LED: 100%; Brightness: 30; Contrast: 50; Colour balance: 50), with at least five images taken per slide. As described by Hall *et al.* (41), histological evidence of necrosis was assessed separately for the epidermis, dermis, hypodermis, panniculus carnosus, and adventitia layers. Features of necrosis included loss of nuclei, nuclear fragmentation (karyorrhexis), nuclear shrinkage and hyperchromasia (pyknosis), loss of cytoplasmic detail with hypereosinophilia, loss of cell borders and, in the case of severe necrosis, disarray with complete loss of architecture and hyalinization. In the epidermis, ulceration with superficial debris was interpreted as evidence of necrosis. In the dermis, loss of skin adnexal structures (e.g., hair follicles and sebaceous glands) and extracellular matrix disarray were also interpreted as evidence of necrosis. The %-necrosis of each skin layer (epidermis, dermis, hypodermis, panniculus carnosus, and adventitia) within each image was assessed by two independent and blinded pathologists and scored between 0 and 4, with 0 meaning no observable necrosis in the layer within that image, 1 meaning up to 25% of the layer in that image exhibiting signs of necrosis, 2 meaning 25-50% necrosis, 3 meaning 50-75%, and 4 meaning more than 75% exhibiting indicators of necrosis. The mean scores of the pathologists for each layer from each image were determined, and the highest scores-per-mouse used for our data analysis as these represented the maximum necrotic severity within each lesion. The ‘dermonecrosis severity score’ was determined for each lesion by taking the mean of the individual layer scores.

Statistical analysis

All data are presented as mean average \pm standard deviation of at least three independent experimental replicates. For cell experiments, ‘n’ is defined as an independent experiment completed at a separate time from other ‘n’s within that group of experiments; all drug and/or venom treatments within an ‘n’ were completed in triplicate wells and the mean taken as the final value for that one trial. For *in vivo* experiments, ‘n’ is defined as the number of mice in that specific treatment group. Two-tailed t-tests were performed for dual comparisons, one-way analysis of variances (ANOVAs) performed for multiple comparisons with one independent variable followed by Dunnett’s or Tukey’s multiple comparisons tests when the trial data were compared to a single control group or to all other groups, respectively, as recommended by GraphPad Prism, and two-way ANOVAs performed for multiple comparisons with two independent variables followed by Dunnett’s multiple comparisons tests. A difference was considered statistically significant where $P \leq 0.05$.

References

1. J. M. Gutiérrez *et al.*, Snakebite envenoming. *Nature Reviews Disease Primers* **3**, 17063 (2017).
2. World Health Organization (WHO). *Snakebite envenoming: a strategy for prevention and control*. Available from: <https://www.who.int/publications/i/item/9789241515641> (Geneva, 2019).

3. C. C. Liu *et al.*, Pathogenesis of local necrosis induced by *Naja atra* venom: Assessment of the neutralization ability of Taiwanese freeze-dried neurotoxic antivenom in animal models. *PLoS Neglected Tropical Diseases* **14**, e0008054 (2020).
4. J. Slagboom, J. Kool, R. A. Harrison, N. R. Casewell, Haemotoxic snake venoms: their functional activity, impact on snakebite victims and pharmaceutical promise. *British Journal of Haematology* **177**, 947-959 (2017).
5. M. D. Coombs *et al.*, Snake bites in Kenya: a preliminary survey of four areas. *Transactions of the Royal Society of Tropical Medicine and Hygiene* **91**(3),319-21 (1997).
6. D. A. Warrell, in *Clinical Toxicology of Animal Venoms and Poisons*, J. Meier, J. White, Eds. (CRC Press, Boca Raton, Florida, 1995), chap. 26, pp. 436-438; 455-492.
7. D. A. Warrell, B. M. Greenwood, N. M. Davidson, L. D. Ormerod, C. R. Prentice, Necrosis, haemorrhage and complement depletion following bites by the spitting cobra (*Naja nigricollis*). *The Quarterly Journal of Medicine* **45**, 1-22 (1976).
8. G. I. Ooms *et al.*, The Burden of Snakebite in Rural Communities in Kenya: A Household Survey. *The American journal of tropical medicine and hygiene* **105**(3), 828–836 (2021).
9. L. T. Erickson *et al.*, The 'Snake song': a pilot study of musical intervention in Eswatini. *Rural and Remote Health* **20**(3), 5494 (2020).
10. World Health Organization (WHO). *Guidelines for the Prevention and Clinical Management of Snakebite in Africa*. Available from: <https://apps.who.int/iris/handle/10665/204458> [online: accessed 18 December 2018] (2010).
11. A. G. Habib *et al.*, Snakebite is Under Appreciated: Appraisal of Burden from West Africa. *PLoS Neglected Tropical Diseases* **9**, e0004088 (2015).
12. T. Tasoulis, G. K. Isbister, A Review and Database of Snake Venom Proteomes. *Toxins*, **9**(9), 290 (2017).
13. A. G. Konshina, I. A. Boldyrev, Y. N. Utkin, A. V. Omel'kov, R. G. Efremov, Snake cytotoxins bind to membranes via interactions with phosphatidylserine head groups of lipids. *PloS One* **6**, e19064 (2011).
14. S. E. Gasanov, R. K. Dagda, E. D. Rael, Snake venom cytotoxins, phospholipase A2s, and Zn²⁺-dependent metalloproteinases: mechanisms of action and pharmacological relevance. *Journal of Clinical Toxicology* **4**, 1000181 (2014).
15. A. V. Feofanov *et al.*, Comparative study of structure and activity of cytotoxins from venom of the cobras *Naja oxiana*, *Naja kaouthia*, and *Naja haje*. *Biochemistry* **69**, 1148-1157 (2004).
16. I. Méndez , J. M. Gutiérrez , A. Angulo , J. J. Calvete , B. Lomonte, Comparative study of the cytolytic activity of snake venoms from African spitting cobras (*Naja* spp., Elapidae) and its neutralization by a polyspecific antivenom. *Toxicon* **58**, 558-564 (2011).
17. E. Kandiwa, B. Mushonga, A. Samkange, E. Fabiano, Quantitative Characterization of the Hemorrhagic, Necrotic, Coagulation-Altering Properties and Edema-Forming Effects of Zebra Snake (*Naja nigricincta nigricincta*) Venom. *Journal of Toxicology* **2018**, 6940798 (2018).
18. S. Chwetzoff, S. Tsunasawa, F. Sakiyama, A. Ménez, Nigexine, a phospholipase A2 from cobra venom with cytotoxic properties not related to esterase activity. Purification, amino acid sequence, and biological properties. *Journal of Biological Chemistry* **264**, 13289-13297 (1989).
19. H. P. Chong, K. Y. Tan, N. H. Tan, C. H. Tan, Exploring the Diversity and Novelty of Toxin Genes in *Naja sumatrana*, the Equatorial Spitting Cobra from Malaysia through De Novo Venom-Gland Transcriptomics. *Toxins* **11**(2), 104 (2019).
20. Y. Liu *et al.*, Cytotoxin 1 from *Naja atra* Cantor venom induced necroptosis of leukemia cells. *Toxicon* **165**, 110-115 (2019).
21. T. D. Kazandjian *et al.*, Convergent evolution of pain-inducing defensive venom components in spitting cobras. *Science* **371**(6527), 386-390 (2021).

22. R. Ralph *et al.*, The timing is right to end snakebite deaths in South Asia. *BMJ* **364**, k5317 (2019).
23. R. M. Kini, S. S. Sidhu, A. H. Laustsen, Biosynthetic Oligoclonal Antivenom (BOA) for Snakebite and Next-Generation Treatments for Snakebite Victims. *Toxins* **10**, 534 (2018).
24. P. Malasit *et al.*, Prediction, prevention, and mechanism of early (anaphylactic) antivenom reactions in victims of snake bites. **292**(6512), 17-20 (1986).
25. N. Sharma, S. Chauhan, S. Faruqi, P. Bhat, S. Varma, Snake envenomation in a north Indian hospital. *Emergency medicine journal* **22**, 118-120 (2005).
26. O. Ogunfowokan, Bite-to-hospital time and morbidity in victims of viper bite in a rural hospital in Nigeria. *African Journal of Primary Health Care & Family Medicine* **4**(1), 371 (2012).
27. C. C. Lin, C. H. Chaou, S. Y. Gao, Influential Factors of Local Tissue Necrosis after Taiwan Cobra Bites: A Secondary Analysis of the Clinical Significance of Venom Detection in Patients of Cobra Snakebites. *Toxins* **13**, 338 (2021).
28. Y. C. Mao *et al.*, *Naja atra* snakebite in Taiwan. *Clinical Toxicology* **56**, 273-280 (2017).
29. W. Bryan-Quiros, J. Fernandez, J. M. Gutierrez, M. R. Lewin, B. Lomonte, Neutralizing properties of LY315920 toward snake venom group I and II myotoxic phospholipases A2. *Toxicon* **157**, 1-7 (2019).
30. M. R. Lewin, T. C. Bulfone, Varespladib (LY315920) rescues mice from rapidly lethal doses of venoms from five vipers, suggesting direct and indirect mechanisms for its therapeutic effect in a mouse model of snakebite envenomation. *Toxicon* **158**, 106289 (2019).
31. M. R. Lewin, S. Samuel, J. Merkel, P. Bickler, Varespladib (LY315920) Appears to Be a Potent, Broad-Spectrum, Inhibitor of Snake Venom Phospholipase A2 and a Possible Pre-Referral Treatment for Envenomation. *Toxins* **8**(9), 248 (2016).
32. D. Petras *et al.*, Snake Venomics of African Spitting Cobras: Toxin Composition and Assessment of Congeneric Cross-Reactivity of the Pan-African EchiTAb-Plus-ICP Antivenom by Antivenomics and Neutralization Approaches. *Journal of Proteome Research* **10**, 1266–1280 (2011).
33. G. Fotakis, J. A. Timbrell, *In vitro* cytotoxicity assays: Comparison of LDH, neutral red, MTT and protein assay in hepatoma cell lines following exposure to cadmium chloride. *Toxicology Letters* **160**, 171–177 (2006).
34. T. Mosmann, Rapid colorimetric assay for cellular growth and survival: application to proliferation and cytotoxicity assays. *Journal of Immunological Methods* **65**, 55-63 (1983).
35. B. S. Cummings, L. P. Wills, R. G. Schnellmann, Measurement of Cell Death in Mammalian Cells. *Current Protocols in Pharmacology* **12**(12.8) (2012).
36. R. D. G. Theakston, H. A. Reid, Development of simple standard assay procedures for the characterization of snake venoms. *Bulletin of the World Health Organization* **61**, 949-956 (1983).
37. L. A. Calderon *et al.*, Antitumoral activity of snake venom proteins: new trends in cancer therapy. *BioMed Research International* **2014**, 203639 (2014).
38. A. Sánchez *et al.*, Comparative venomics and preclinical efficacy evaluation of a monospecific *Hemachatus* antivenom towards sub-Saharan Africa cobra venoms. *Journal of Proteomics* **240**, 104196 (2021).
39. F. A. Adamude *et al.*, Proteomic analysis of three medically important Nigerian *Naja* (*Naja haje*, *Naja katiensis* and *Naja nigricollis*) snake venoms. *Toxicon* **197**, 24-32 (2021).
40. W. Laprade *et al.*, Machine-learning guided Venom Induced Dermonecrosis Analysis tool: VIDAL [preprint]. *bioRxiv*, DOI: 10.1101/2023.05.21.541619 (2023).
41. S. R. Hall *et al.*, Repurposed drugs and their combinations prevent morbidity-inducing dermonecrosis caused by diverse cytotoxic snake venoms [preprint]. *bioRxiv*, DOI: 10.1101/2022.05.20.492855 (2022).

42. M. Karakas, W. Koenig, Varespladib methyl, an oral phospholipase A2 inhibitor for the potential treatment of coronary artery disease. *IDrugs* **12**(9), 585-92 (2009).
43. R. S. Rosenson, H. Fraser, J. Trias, C. Hislop, Varespladib methyl in cardiovascular disease. *Expert opinion on investigational drugs* **19**(10), 1245-55 (2010).
44. K. E. Suckling, Phospholipase A2 inhibitors in the treatment of atherosclerosis: a new approach moves forward in the clinic. *Expert opinion on investigational drugs* **18**(10), 1425-30 (2009).
45. M. R. Lewin *et al.*, Varespladib in the Treatment of Snakebite Envenoming: Development History and Preclinical Evidence Supporting Advancement to Clinical Trials in Patients Bitten by Venomous Snakes. *Toxins* **14**(11), 783 (2022).
46. Y. Wang *et al.*, Exploration of the Inhibitory Potential of Varespladib for Snakebite Envenomation. *Molecules* **23**(2), 391 (2018).
47. H. Xiao *et al.*, Inactivation of Venom PLA2 Alleviates Myonecrosis and Facilitates Muscle Regeneration in Envenomed Mice: A Time Course Observation. *Molecules* **23**(8), 1911 (2018).
48. A. S. Arias, A. Rucavado, J. M. Gutierrez, Peptidomimetic hydroxamate metalloproteinase inhibitors abrogate local and systemic toxicity induced by *Echis ocellatus* (saw-scaled) snake venom. *Toxicon* **132**, 40-49 (2017).
49. C. Knudsen *et al.*, Novel Snakebite Therapeutics Must Be Tested in Appropriate Rescue Models to Robustly Assess Their Preclinical Efficacy. *Toxins* **12**, 528 (2020).
50. J. M. Stringer, R. A. Kainer, A. T. Tu, Ultrastructural studies of myonecrosis induced by cobra venom in mice. *Toxicology and applied pharmacology* **18**, 442-450 (1971).
51. C. L. Ownby, J. E. Fletcher, T. R. Colberg, Cardiotoxin 1 from cobra (*Naja naja atra*) venom causes necrosis of skeletal muscle *in vivo*. *Toxicon* **31**, 697-709 (1993).
52. J. M. Gutiérrez *et al.*, Pan-African polyspecific antivenom produced by caprylic acid purification of horse IgG: an alternative to the antivenom crisis in Africa. *Transactions of the Royal Society of Tropical Medicine and Hygiene* **99**, 468-475 (2005).
53. S. Sanhajariya, S. B. Duffull, G. K. Isbister, Investigating myotoxicity following Australian red-bellied black snake (*Pseudechis porphyriacus*) envenomation. *PloS one* **16**(9), e0256653 (2021).
54. A. Kasturiratne *et al.*, The Global Burden of Snakebite: A Literature Analysis and Modelling Based on Regional Estimates of Envenoming and Deaths. *PLoS Medicine*, **5**(11):e218 (2008).
55. A. G. Habib, Public health aspects of snakebite care in West Africa: perspectives from Nigeria. *Journal of Venomous Animals and Toxins including Tropical Diseases* **19**(1), 27 (2013).
56. S. Waiddyanatha, A. Silva, S. Siribaddana, G. K. Isbister, Long-term Effects of Snake Envenoming. *Toxins* **11**(4), 193 (2019).
57. B. Lomonte *et al.*, Comparative study of the cytolytic activity of myotoxic phospholipases A2 on mouse endothelial (tEnd) and skeletal muscle (C2C12) cells *in vitro*. *Toxicon* **37**, 145-158 (1999).
58. P. E. Bougis, P. Marchot, H. Rochat, *In vivo* synergy of cardiotoxin and phospholipase A2 from the elapid snake *Naja mossambica mossambica*. *Toxicon* **25**, 427-431 (1987).
59. N. H. Tan, A. Armugam, *In vivo* interactions between neurotoxin, cardiotoxin and phospholipases A2 isolated from Malayan cobra (*Naja naja sputatrix*) venom. *Toxicon* **28**, 1193-1198 (1990).
60. R. Doley, R. M. Kini, Protein complexes in snake venom. *Cellular and Molecular Life Sciences* **66**, 2851-2871 (2009).
61. K. H. Slotta, J. A. Vick, Identification of the direct lytic factor from cobra venom as cardiotoxin. *Toxicon* **6**, 167-168 (1969).

62. M. Rivel *et al.*, Pathogenesis of dermonecrosis induced by venom of the spitting cobra, *Naja nigricollis*: An experimental study in mice. *Toxicon* **119**, 171-117 (2016).
63. C. Xie *et al.*, Varespladib Inhibits the Phospholipase A2 and Coagulopathic Activities of Venom Components from Hemotoxic Snakes. *Biomedicines* **8**, 165 (2020).
64. T. D. Kazandjian *et al.*, Anticoagulant Activity of *Naja nigricollis* Venom Is Mediated by Phospholipase A2 Toxins and Inhibited by Varespladib. *Toxins* **13**, 302 (2021).
65. N. R. Casewell, T. N. W. Jackson, A. H. Laustsen, K. Sunagar, Causes and Consequences of Snake Venom Variation. *Trends in Pharmacological Sciences* **41**, 570-581 (2020).
66. S. J. Nicholls *et al.*, Varespladib and cardiovascular events in patients with an acute coronary syndrome: the VISTA-16 randomized clinical trial. *JAMA* **311**, 252-262 (2014).
67. T. H. Baryakova, B. H. Pogostin, R. Langer, K. J. McHugh, Overcoming barriers to patient adherence: the case for developing innovative drug delivery systems. *Nature Reviews Drug Discovery* **22**, 387-409 (2023).
68. N. Tiwari, G. Aggarwal, G. K. Jain, G. Mittal, Multi-drug loaded microneedles for emergency treatment of snakebite envenomation. *Medical Hypotheses* **165**, 110908 (2022).
69. M. Abouyannis *et al.*, Paediatric snakebite in Kilifi County, Kenya: A 19-year observational study [preprint]. *medRxiv*, DOI: 10.1101/2022.11.28.22282866 (2022).
70. E. M. Landis, The Capillaries of the Skin: A Review. *Journal of Investigative Dermatology* **1** (4), 295-311, (1938).
71. Techniques in the Behavioral and Neural Sciences, 2 - *Intravenous Drug Administration*. V. Claassen, Ed., Techniques in the Behavioral and Neural Sciences (Elsevier, 1994), vol. 12.
72. H. Sun, Y. X. Zhang, Y. M. Li, Generation of Skin Organoids: Potential Opportunities and Challenges. *Frontiers in Cell and Developmental Biology* **9**, 709824 (2021).
73. S. Saeidnia, A. Manayi, M. Abdollahi, From in vitro Experiments to in vivo and Clinical Studies; Pros and Cons. *Current Drug Discovery Technologies* **12**(4), 218-24 (2015).
74. R. L. Perlman, Mouse models of human disease: An evolutionary perspective. *Evol Med Public Health* **1**, 170-176 (2016).
75. V. W. Wong, M. Sorkin, J. P. Glotzbach, M. T. Longaker, G. C. Gurtner, Surgical approaches to create murine models of human wound healing. *Journal of Biomedicine & Biotechnology* **2011**, 969618 (2011).
76. D. N. Perkins, D. J. Pappin, D. M. Creasy, J. S. Cottrell, Probability-based protein identification by searching sequence databases using mass spectrometry data. *Electrophoresis: An International Journal* **20**, 3551-3567 (1999).
77. V. G. Wilson, Growth and differentiation of HaCaT keratinocytes. *Methods in Molecular Biology* **1195**, 33-41 (2014).
78. I. Colombo *et al.*, HaCaT Cells as a Reliable *In Vitro* Differentiation Model to Dissect the Inflammatory/Repair Response of Human Keratinocytes. *Mediators of Inflammation* **2017**, 7435621 (2017).
79. T. P. Jenkins *et al.*, AHA: AI-guided tool for the quantification of venom-induced haemorrhage in mice. *Frontiers in Tropical Diseases* **3**, 1063640 (2022).

Acknowledgments

The authors thank Paul Rowley for maintenance of snakes and provision of venom, Dr. Cassandra Modahl and Dr. Amy Marriott for assistance with animal welfare observations during *in vivo* experimentation, Valerie Tilston and colleagues at the University of Liverpool for preparing histopathology slides, and Dr. Matt Lewin for provision of varespladib. The authors acknowledge use of the Biomedical Services Unit provided by Liverpool Shared Research Facilities, Faculty of Health and Life Sciences, University of Liverpool.

Funding:

Funding for this study was provided by:

- (i) A Newton International Fellowship (NIF\R1\192161) from the Royal Society to SRH,
- (ii) A Sir Henry Dale Fellowship (200517/Z/16/Z) jointly funded by the Wellcome Trust and the Royal Society to NRC,
- (iii) Wellcome Trust funded grants (221712/Z/20/Z and 221708/Z/20/Z) to RAH and NRC,
- (iv) UK Medical Research Council research grants (MR/S00016X/1 and MR/L01839X/1) to RAH, J-MG and NRC and,
- (v) A UK Medical Research Council funded Confidence in Concept Award (MC_PC_15040) to NRC.

This research was funded in part by the Wellcome Trust. For the purpose of open access, the authors have applied a CC BY public copyright licence to any Author Accepted Manuscript version arising from this submission.

Author contributions:

Conceptualisation: KEB, SRH, JMG, NRC

Methodology: KEB, SRH, SAR, WL, TPJ, MCW, JMG, NRC

Investigation: KEB, SRH, SAR, EC, CAD, L-OA, WL, RAH, AJS, TPJ, MCW, JMG, NRC

Data curation: KEB, SRH, SAR, WL, TPJ, JMG, NRC

Formal analysis: KEB, SRH, SAR, AJS, MCW, JMG, NRC

Original draft preparation: KEB, SRH, JMG, NRC

Editing: All authors

Competing interests: Authors declare no competing interests.

Data and materials availability: All data needed to evaluate the conclusions in the paper are present in the paper, the Supplementary Materials, or via the publicly available FigShare repository: 10.6084/m9.figshare.23580120.

Supplementary Materials

Figs. S1 to S11

Tables S1 to S3

Data S1

Supplementary Materials for

Dermonecrosis caused by spitting cobra snakebite is the result of toxin potentiation and is prevented by the repurposed drug varespladib

Keirah Bartlett *et al.*

*Corresponding author. Email: nicholas.casewell@lstmed.ac.uk

The Supplementary Material includes:

Figs. S1 to S11
Tables S1 to S3

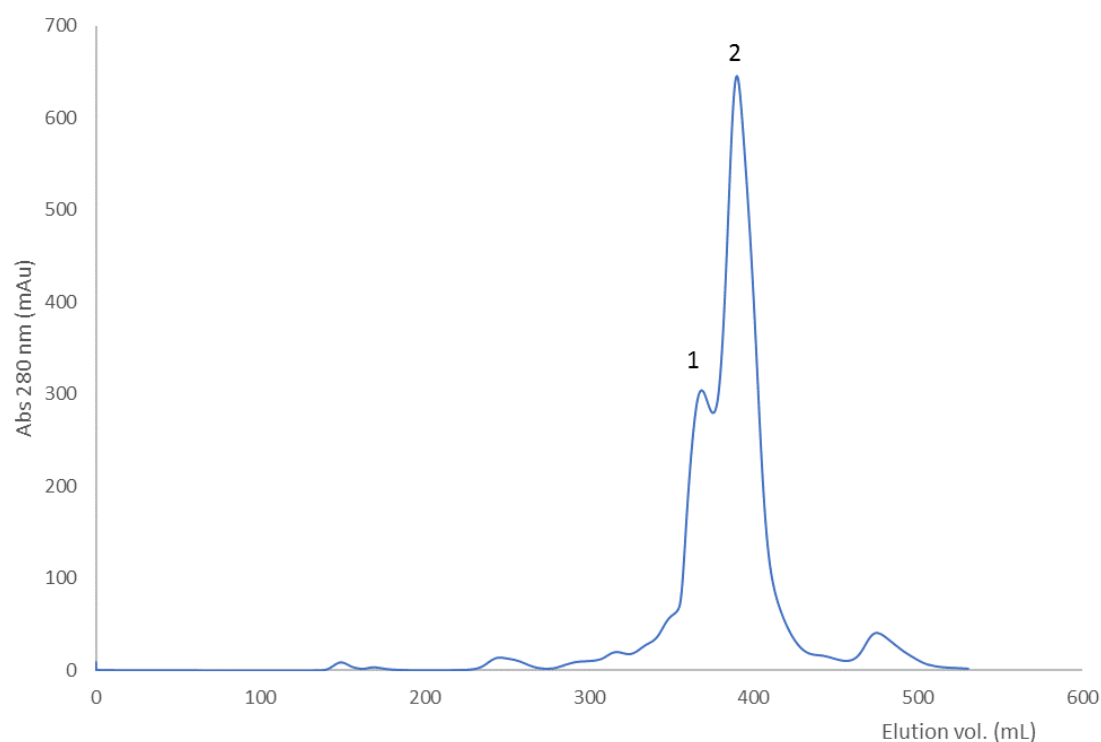


Fig. S1. Gel filtration chromatography of whole venom.

100 mg of *N. nigricollis* (Tanzania) venom was dissolved in 5 mL PBS and centrifuged prior to separation. This was loaded onto a 480 mL column of Superdex 200HR equilibrated in PBS. The column was operated at a flow rate of 2.0 mL/min and elution was monitored at 280 nm. The overlapping peaks for PLA₂ and 3FTX are numbered 1 and 2 respectively. These were pooled and then subjected to cation exchange chromatography (see Fig. S2).

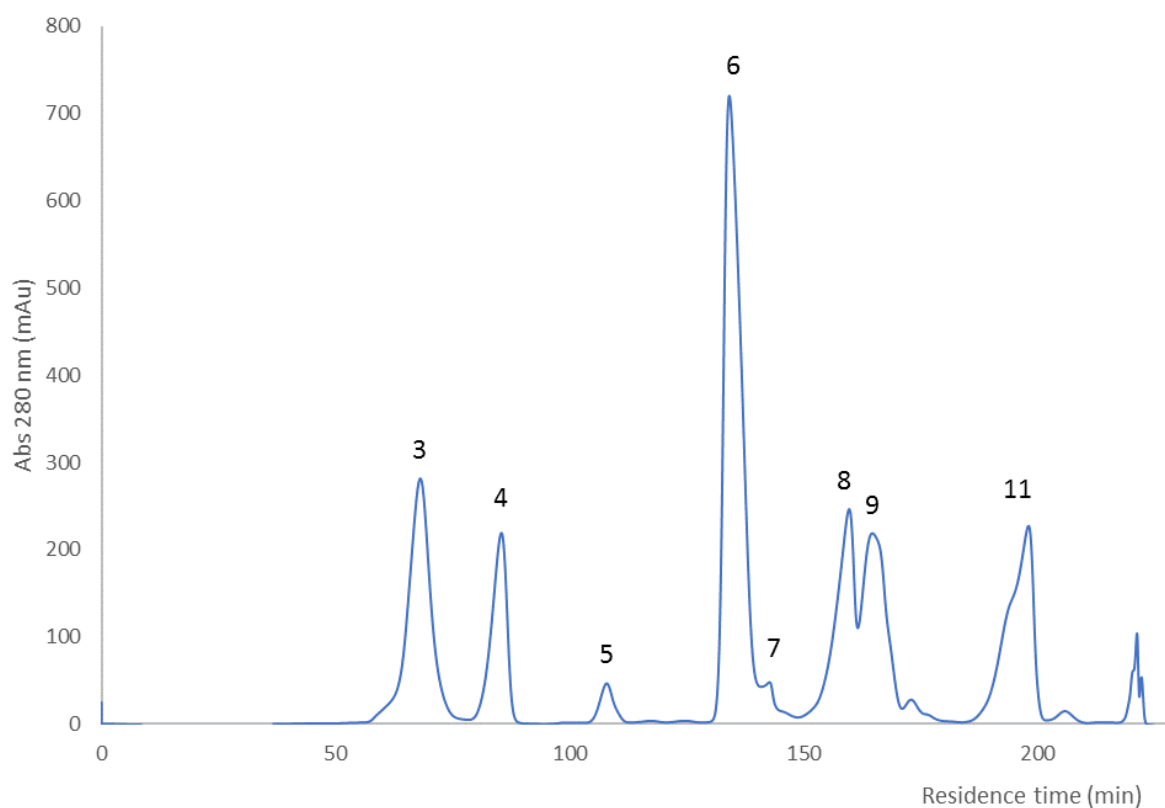


Fig. S2. Cation exchange chromatography of the PLA₂ and 3FTX fraction from GFC.

Peaks 1 and 2 from GFC were pooled and dialysed against 50 mM sodium phosphate, pH 6.0 and then applied to a 20 mL HPSP column equilibrated in the same buffer. Elution was carried using a 15 CV gradient of 0 - 0.7 M NaCl in 50 mM sodium phosphate, pH 6.0. Flow rate was 1.5 mL/min and elution was monitored at 280 nm. Peak 4 contained pure acidic PLA₂ (named acidic PLA₂ 2). The major peaks, labelled 3, 6, 8, 9, and 11 were subject to further chromatographic steps.

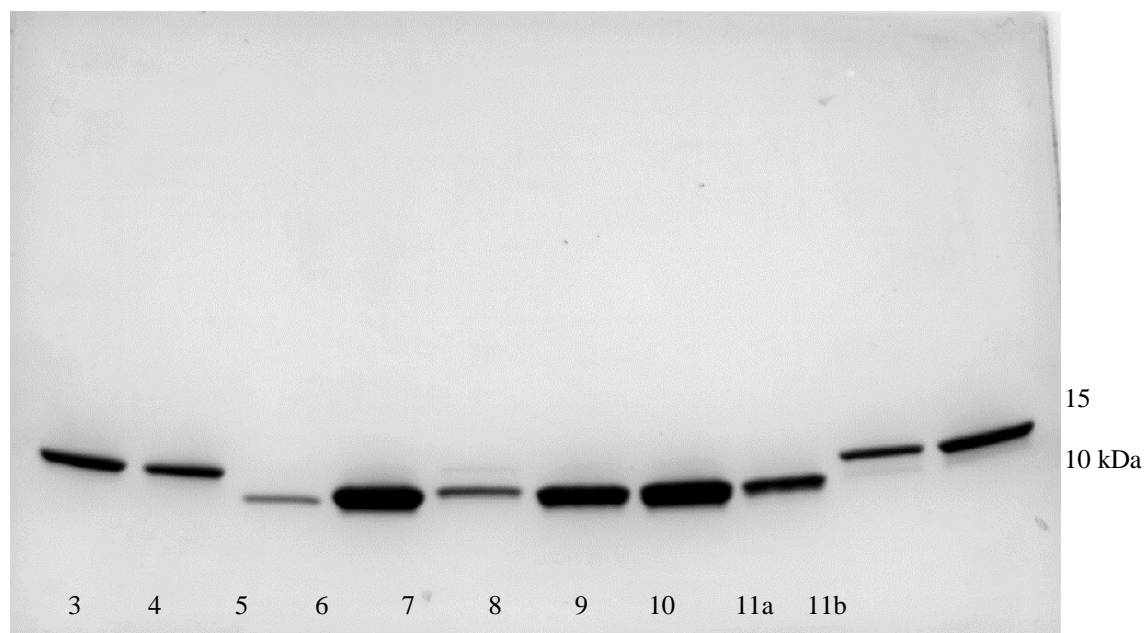


Fig. S3. SDS-PAGE analysis of peaks from cation exchange chromatography.

Seven μL samples were loaded onto 4-20% acrylamide gels (BioRad) and run using the Tris-glycine buffer system under reducing conditions. The gels were subsequently stained with Coomassie Blue R250. The position of relevant molecular weight markers is shown on the right (kDa). Chromatography peak numbers are indicated at the base of the figure. Peak 11 was run as two fractions, a and b, reflecting the wide asymmetric peak shape. Peak 10 contained overlapping material from peak 9, hence the band intensity is greater than would be expected for the height of peak 10.

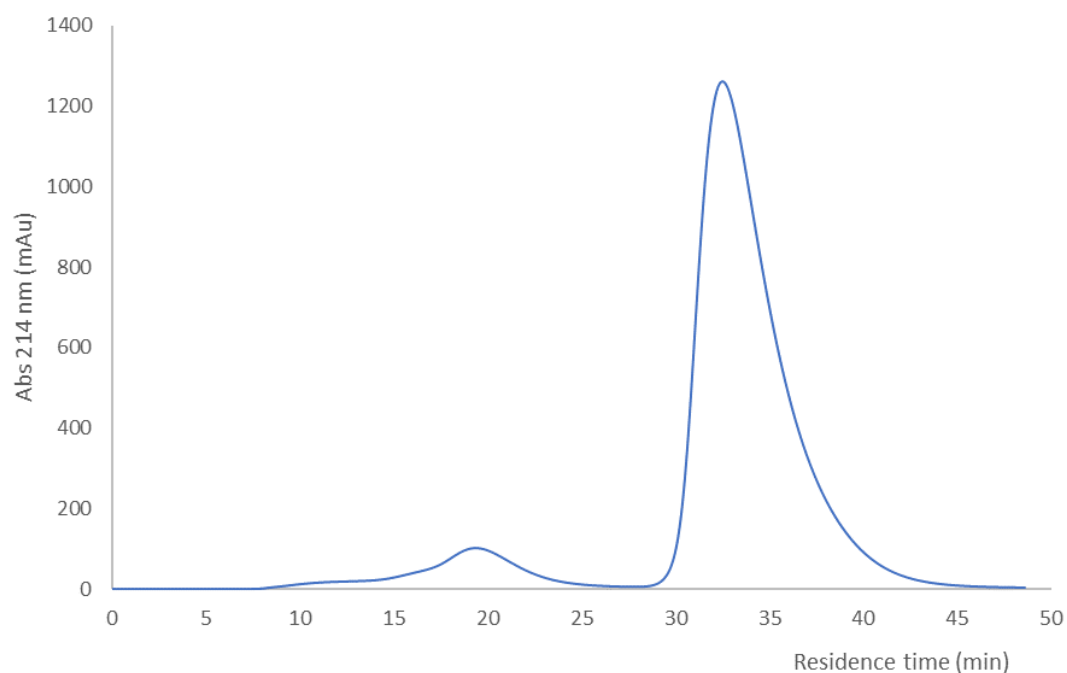


Fig. S4. Hydrophobic interaction chromatography of acidic PLA₂ (peak 3).

Peak 3 from the cation exchange chromatography step was loaded directly onto a 4.7 mL column of Phenyl Sepharose LS FF equilibrated in 25 mM sodium phosphate pH 7.2. Elution was carried out with a 0-100% (4CV) gradient of 25 mM sodium phosphate pH 7.2 to 25% ethanol in 25 mM sodium phosphate pH 7.2. The column was operated at 1.0 mL/min and elution was monitored at 214 nm.

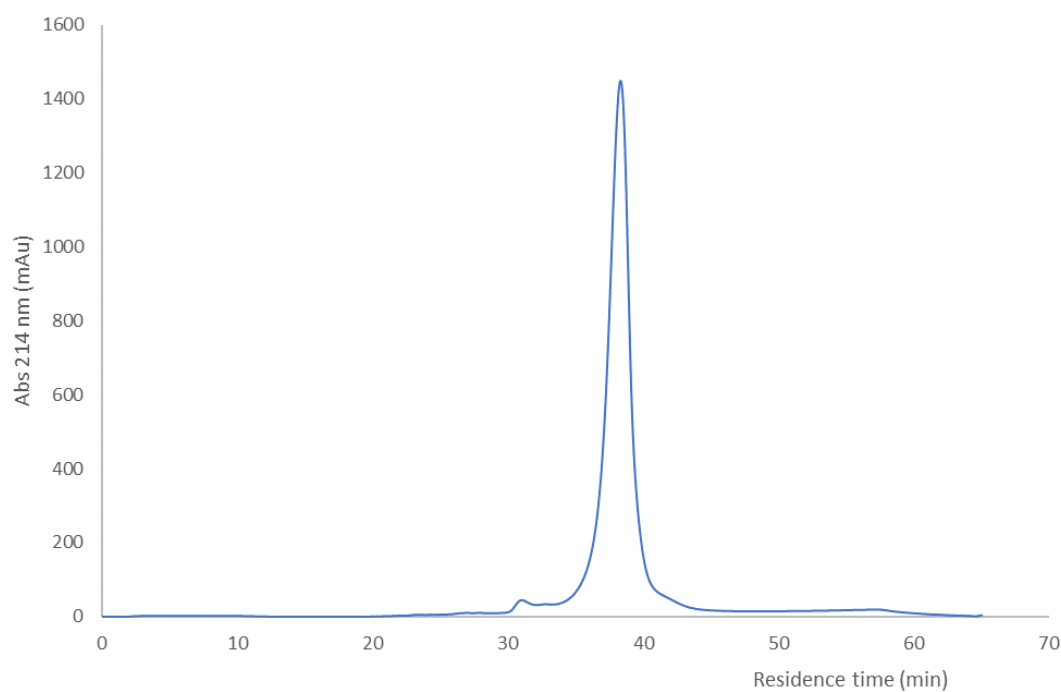


Fig. S5. Hydroxyapatite chromatography of basic PLA₂ (peak 11).

Peak 11 from the cation exchange chromatography step was dialysed against 5 mM sodium phosphate pH 6.8 and then loaded onto a 1 mL column of ceramic hydroxyapatite (CHT I) equilibrated in the same buffer. Using a flow rate of 0.5 mL/min, elution was carried out with gradient of 5 mM sodium phosphate pH 6.8 to 500 mM sodium phosphate pH 6.8, 0.15 M NaCl over 20 CV. Elution was monitored at 214 nm.

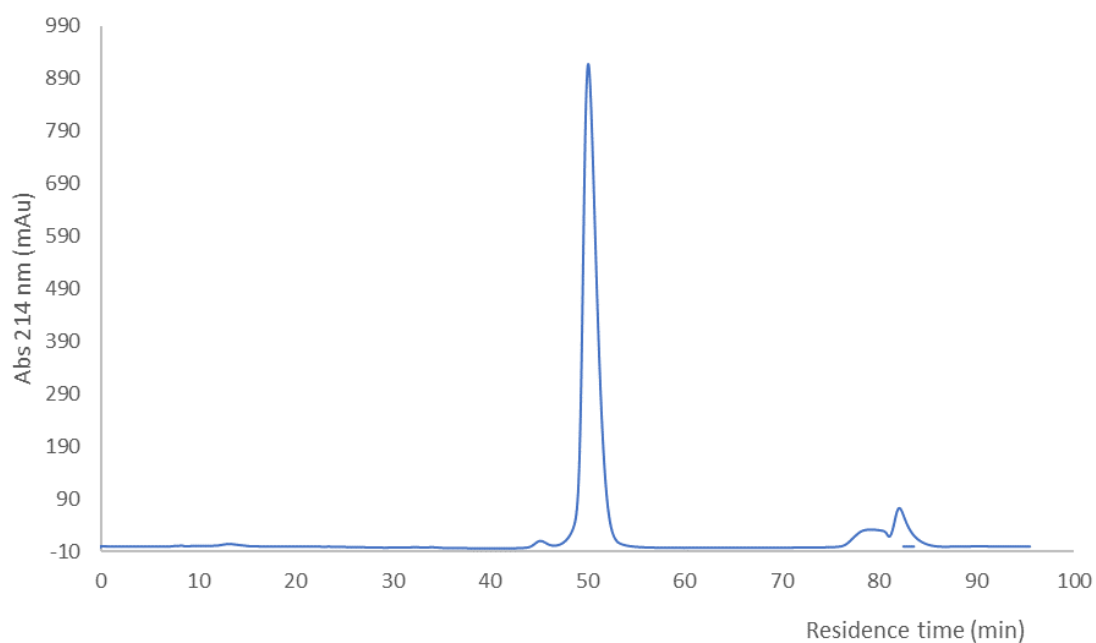


Fig. S6. Hydrophobic interaction chromatography of peak 6 3FTx cytotoxin 1.

The material in peak 6 from cation exchange chromatography was made to 1.5 M in NaCl and loaded onto a 10 mL Phenyl Superose column. Proteins were then eluted in a 5 CV gradient of 1.5 M NaCl in 25 mM sodium phosphate pH 7.2 to 30% (v/v) ethylene glycol in 25 mM sodium phosphate pH 7.2. The flow rate was 1 mL/min and elution was monitored at 214 nm.

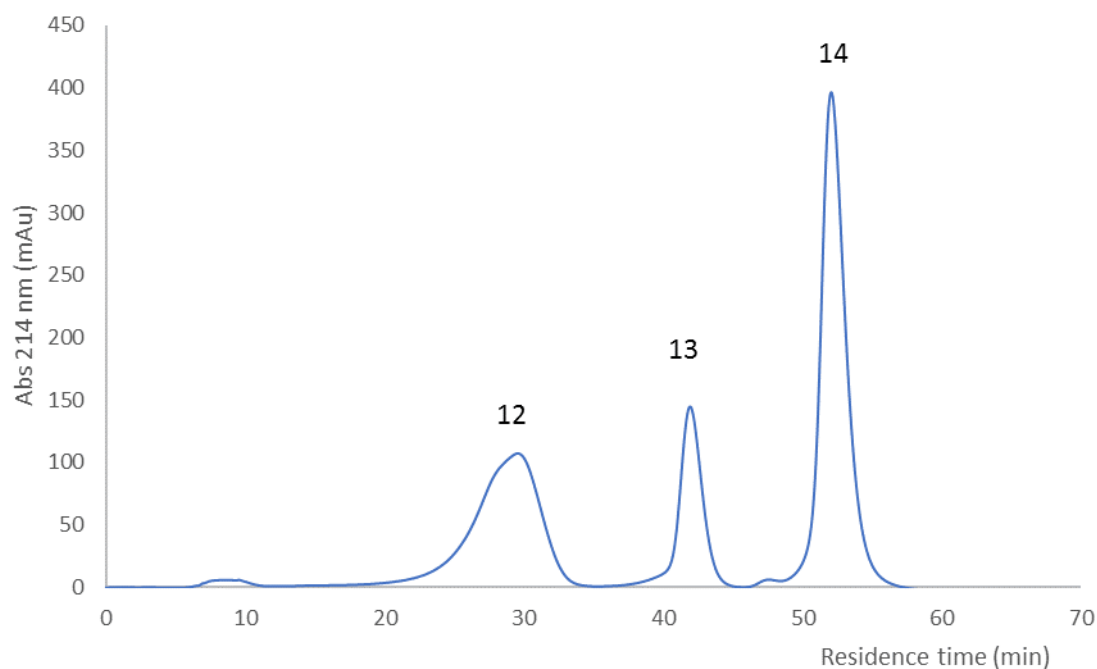


Fig. S7. Hydrophobic interaction chromatography of 3FTx cytotoxins 1v, 3 and 4.

The material in peak 8 and 9 from cation exchange chromatography was made to 1.2 M in NaCl and loaded onto a 10 mL Phenyl Superose column. Proteins were then eluted in a 5 CV gradient of 1.2 M NaCl in 25 mM sodium phosphate pH 7.2 to 30% (v/v) ethylene glycol in 25 mM sodium phosphate pH 7.2. The flow rate was 1 mL/min and elution was monitored at 214 nm. Peak 12, 13 and 14 respectively contained cytotoxin 4, cytotoxin 1v and cytotoxin 3.

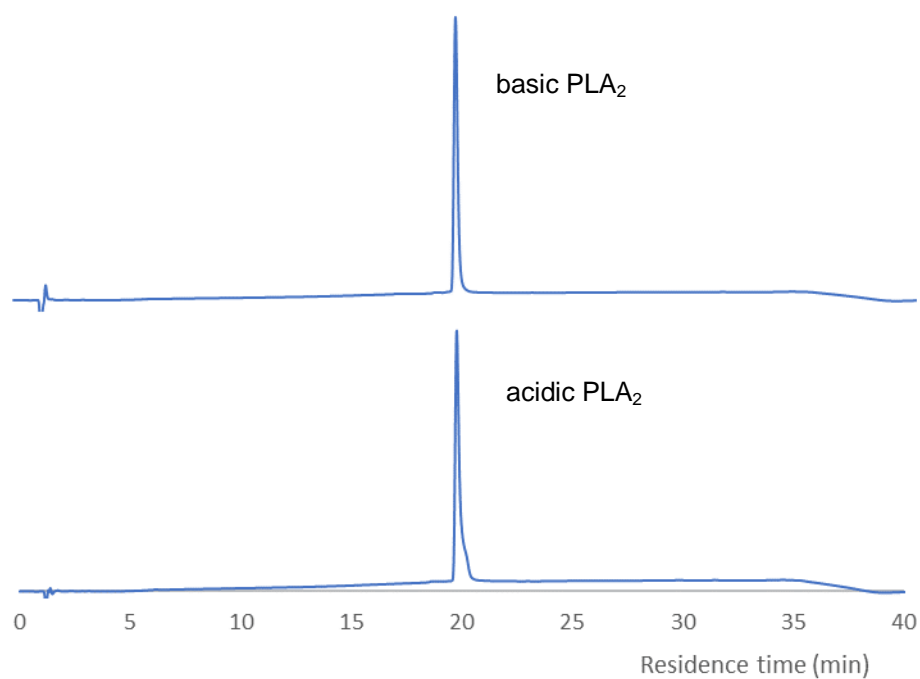


Fig. S8. Analytical RP-HPLC of purified PLA₂s.

RP-HPLC was performed on a Biobasic C4 column (2.1 x 150 mm). The flow rate was 0.2 mL/min and proteins were separated in a gradient of 0-65% acetonitrile in 0.1% trifluoroacetic acid, with monitoring at 214 nm (Y-axis, mAu units not shown). The acidic PLA₂ shown is acidic PLA₂ 1; acidic PLA₂ 2 had an identical profile on RP-HPLC and the two were combined to give the acidic PLA₂ pool used throughout this study.

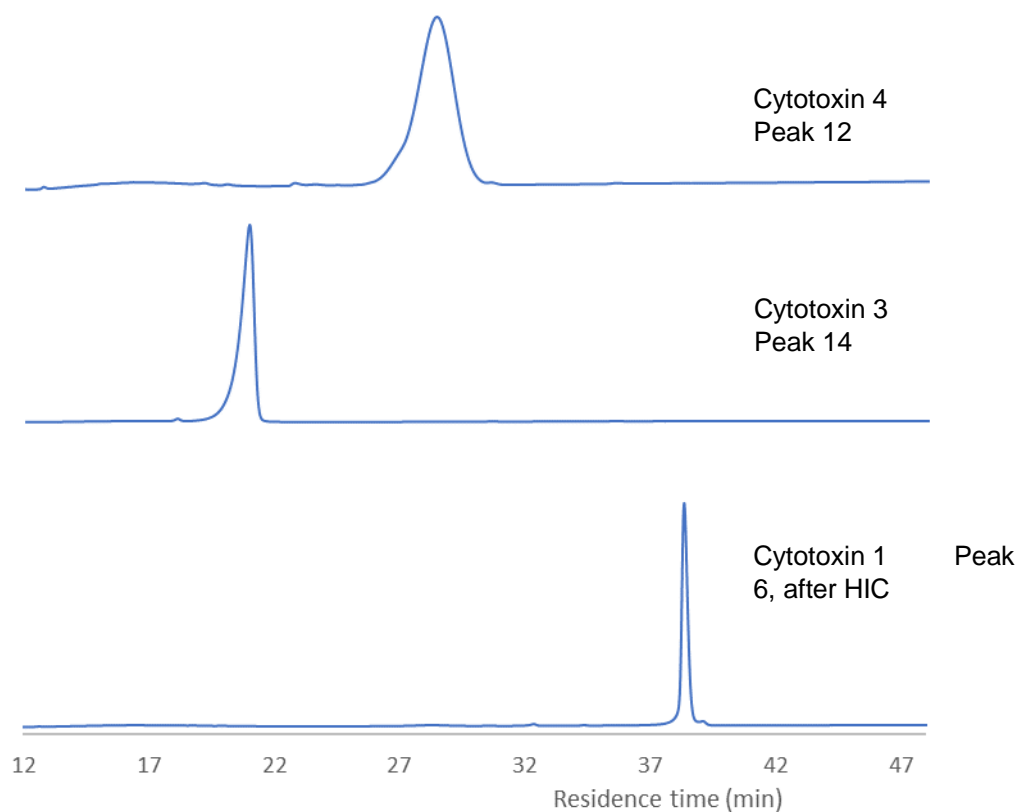


Fig. S9. Analytical RP-HPLC of purified 3FTx cytotoxins 1, 3 and 4.

RP-HPLC was performed on a Biobasic C4 column (2.1 x 150 mm). The flow rate was 0.2 mL/min and proteins were separated in a gradient of acetonitrile (0-25%/5 min, 25-50%/30 min, 50-90%/5 min) in 0.1% trifluoroacetic acid, with monitoring at 214 nm (Y-axis, mAu units not shown).

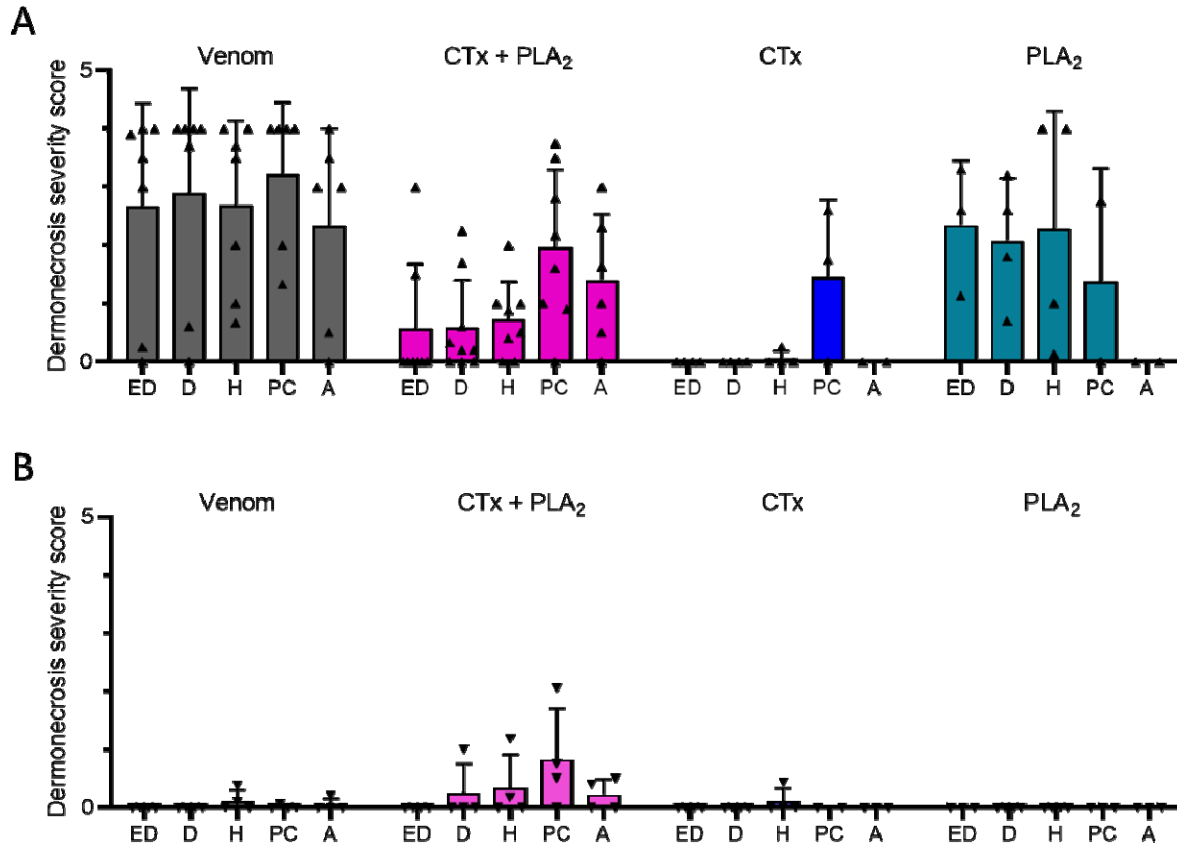


Fig. S10. Histopathological analysis of dermonecrotic skin lesions shows that microscopic pathology caused by *N. nigricollis* venom is prevented by the PLA₂ inhibitor varespladib.

A) Histopathology analysis resulting in dermonecrosis severity scores for multiple skin layers are shown following intradermal dosing of mice with crude East African (Tanzania) *N. nigricollis* venom, the CTX + PLA₂ combination, and CTXs and PLA₂s separately. Key: ED, epidermis; D, dermis; H, hypodermis; PC, panniculus carnosus; A, adventitia. **B)** Co-injection of mice with the PLA₂ inhibitor varespladib significantly reduces damage scores across multiple skin layers. Data shown represents the mean damage score for each skin layer and error bars represent the corresponding standard deviations.

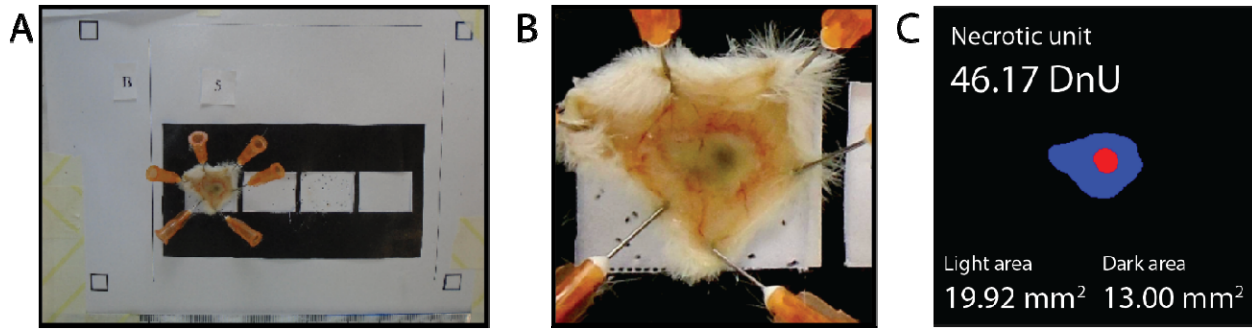


Fig. S11. Overview of the VIDAL workflow. First, **A**) the raw image is imported and automatically standardised. Thereafter, **B**) the lesion is identified and cropped out for further analysis. Finally, **C** the processed image is segmented and light and dark lesions automatically identified. This information is used to calculate dermonecrotic units (DnUs) for each identified lesion, with a 2:1 weighting of dark to light lesion areas.

Table S1. Summary of MS analysis and identification of the purified toxins.

Chromatography peak no.		Intact mass	MS/MS ID					
CatX	HIC	(Mono, Da)	Protein ID	Entry Name	Length	Percent Coverage	Organism	Protein Description
3		13,172	P00602	PA2A1_NAJMO	118	85.6	Naja mossambica OX=8644	Acidic phospholipase A2 CM-I
4		13,287	P00602	PA2A1_NAJMO	118	85.6	Naja mossambica OX=8644	Acidic phospholipase A2 CM-I
11		13,249	P00605	PA2B4_NAJNG	118	93.2	Naja nigricollis OX=8654	Phospholipase A2 'basic'
6		6,818	P01468	3SA1_NAJPA	60	100	Naja pallida OX=8658	Cytotoxin 1
8+9	12	6,707	P01452	3SA4_NAJMO	60	63.3	Naja mossambica OX=8644	Cytotoxin 4
8+9	13	6,817	P01468	3SA1_NAJPA	60	100	Naja pallida OX=8658	Cytotoxin 1
8+9	14	6,884	P0DSN1	3SAN_NAJNG	60	96.7	Naja nigricollis OX=8654	Naniproin [cytotoxin 3]

Table S2. Dermonecrotic lesions from mice dosed with *N. nigricollis* venom and toxins, with and without varespladib.

Mice were intradermally injected with East African (Tanzania) *N. nigricollis* venom (63 μ g), or proportional amounts of purified CTx + PLA₂S (37.8 + 16.4 μ g), purified CTx-only (37.8 μ g), and purified PLA₂S-only (16.4 μ g) either alone, or pre-incubated with the PLA₂-inhibitor varespladib (19 μ g). Mice were culled at 72 h post-injection, lesions excised, and photographs taken. White scale bars represent 5 mm.

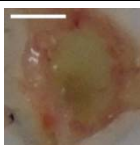
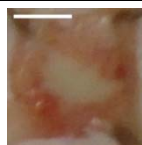
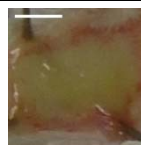
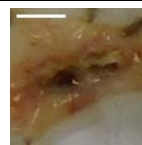
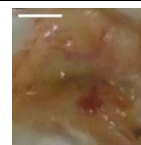
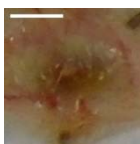
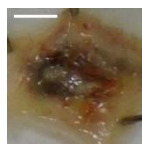








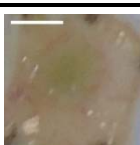

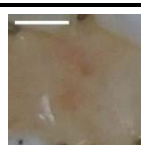
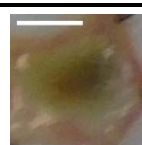


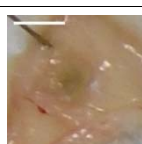

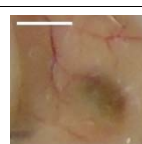



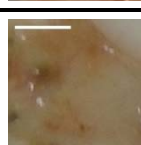


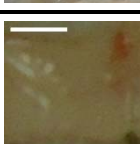
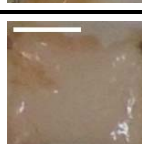
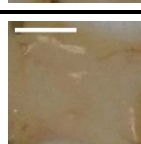








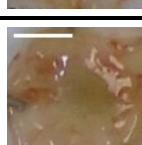

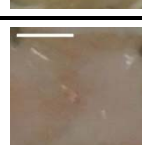

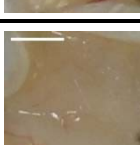




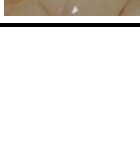
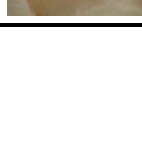
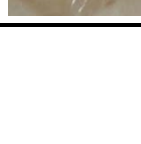
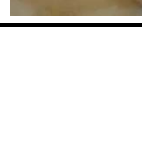
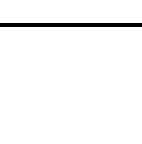
Venom					
					
Venom + varespladib					
					
CTXs + PLA₂S					
					
CTXs + PLA₂S + varespladib					
CTXs-only					
CTXs-only + varespladib					
PLA₂S-only					
PLA₂S + varespladib					

Table S3. Dermonecrotic lesions from mice dosed with *N. pallida* venom, with and without varespladib.

Mice were intradermally injected with *N. pallida* venom (25 µg) either alone, or pre-incubated with the PLA₂-inhibitor varespladib (19 µg). Mice were culled at 72 h post-injection, lesions excised, and photographs taken. White scale bars represent 5 mm.

